ABSTRACT

Title of Thesis: HIGH ACCELERATIONS PRODUCED THROUGH SECONDARY IMPACT AND ITS EFFECT ON RELIABILITY OF PRINTED WIRING ASSEMBLIES

Stuart Taylor Douglas, Master of Science, 2010

Thesis directed by: Professor Abhijit Dasgupta
Department of Mechanical Engineering

The focus of this thesis is the investigation of extremely high accelerations through secondary impact and its effect on reliability of printed wiring assemblies. The test equipment consists of a commercially available drop system and a commercially available attachment termed a Dual Mass Shock Amplifier (DMSA), which extends the impact acceleration range to as much as 30,000 Gs by utilizing secondary impact dynamics. Further secondary impacts between the test vehicle and fixture are intentionally generated in simulation and tested experimentally to imitate board 'slap' phenomena in product assemblies, and to generate even further amplification of the acceleration at various locations on the test specimen.

In this thesis a detailed description of the test equipment and modeling techniques are provided. Model complexity ranges from simple analytic closed-form rigid-body mechanics to detailed nonlinear dynamic finite element analysis. The effects of different equipment design parameters (table mass, spring stiffness, table clearance) are investigated through parametric modeling. The effects of contact parameters (constraint enforcement algorithms, stiffness, damping) on model accuracy are explored. Test fixtures for high shock accelerations are discussed and used for board level reliability testing of printed wire assemblies containing WLCSP49s and MEMS microphones.

HIGH ACCELERATIONS PRODUCED THROUGH SECONDARY IMPACT AND ITS EFFECT ON RELIABILITY OF PRINTED WIRING ASSEMBLIES

by

Stuart Taylor Douglas

Thesis submitted to the Faculty of the Graduate School of the
University of Maryland, College Park in partial fulfillment
of the requirements for the degree of
Mechanical Engineering
Master of Science
2010

Advisory Committee:

Professor Abhijit Dasgupta, Chair/Advisor
Professor Hugh Bruck
Professor Amr Baz

TABLE OF CONTENTS

List of Tables

List of Figures

Acknowledgements

I owe my gratitude to all the people who have helped me succeed in my quest for higher learning.

I would like to especially thank my advisor Professor Abhijit Dasgupta because without his willingness to give someone a chance, none of this would be possible. Like all good teachers, he has high expectations for his students, but was always there to lend a helping hand and willing to get involved no matter the subject. His brilliance, wisdom, kindness, and enthusiasm were always what I needed to persevere in stressful times. I consider him not only a mentor, but also a good friend.

My friends and family deserve to be mentioned as well. First, I would like to thank my friends and co-workers Lynn, Cholmin, Koustav, Gayatri, Dan, Subhassis, Josh, Eshan, Farbod, Nicholas, Arnaud, Abdou, Nick, and the six generations of German interns. I could count on these people for assistance on any problem. Second, infinite thanks go out to my family. Thanks to my parents and brother for the incredible support, financial and otherwise, while I tried to figure out real life. Finally, thanks to Leslie because she was my rock throughout it all.

Special thanks go to Chuck, Markku, Moustafa, and Ryuichi for helping me in my research and being patient while I learned how to work in industry.

Thanks are also due to all my teachers. I really enjoyed the graduate course work at University of Maryland, because teachers enjoyed teaching. It makes all the difference in the world to a student.

To all the people I forgot, it's inevitable, I apologize.

1 Introduction

1.1 Background and motivation

Drop testing has become an integral part of reliability testing of portable electronic products, and is used to simulate impact load conditions that arise in the field. For example, a person that drops an expensive mobile phone onto the ground expects it to work in the same way upon recovery. Therefore, product manufacturers are increasingly turning to reliability tests which will accurately capture the end users' load conditions so that products can be designed to withstand drop conditions. Furthermore, a mobile phone is made up of several subsystems (battery, circuit boards, LCD screens, etc.) and depending on the architecture of these subsystems and magnitude of the impact, collisions between these substructures can occur [1]. These collisions can cause significant amplification of the primary impact event, due to , momentum exchange between masses traveling at opposing velocities (e.g. the phone case and a suspended circuit board), and are termed secondary impacts in this study [2]. While product designers generally do their best to prevent secondary impact between internal structures, they are sometimes inevitable and it is hence important to develop test equipment that can use secondary impacts to reproduce high accelerations and accurately capture these unique application conditions. Extremely high accelerations, such as those produced by secondary impacts, are important for a second reason. These highly severe tests are often useful for testing of structures that are too robust for conventional drop testing recommended by commercial standards like JEDEC.

The literature contains several investigations of high impact accelerations produced through secondary impact in practical applications. As early as the late 1960s, the phenomenon of velocity amplification through multiple impacts between moving bodies, was investigated in several papers. A paper published by Hart and Hermann [3], concluded that the masses of multiple bodies could be optimized such that the ratio between them produced maximum energy transfer [4]. Furthermore, works by Kerwin [5], derived equations for velocity momentum, and kinetic energy, dependent on a coefficient of restitution of zero or one [4]. An investigation by Harter et al. devised an experiment to study successively smaller balls stacked above each other and dropped to the ground [6]. They concluded that the ratio of all the masses could be optimized such that the velocity of all the masses, except the final mass which is linearly dependent with the number of the masses in the system, drop to zero. Askari [2] and Goyal [1] demonstrated that interactions between the subsystems of a handheld product (battery, circuit board, case) can produce velocity impacts.

1.2 Literature review

The sections below will go into a brief review of available literature regarding the topic of the chapter listed in the section heading. Additional literature will be provided at the start of each chapter if required.

1.2.1 Simulation of secondary contact to generate very high accelerations

Chapter 2 of this thesis is solely dedicated to investigating a commercial drop tower and a mechanical acceleration amplifier. Design of this system is parametrically explored, based on transient finite element analysis and experiments. Recent work by Rodgers et al. [4], have derived guidelines for building test machines to provide velocity

amplification by secondary impacts. Their work [7], concluded that the velocity of the largest falling mass, in a system of successively smaller masses stacked up on top of each other, can be amplified as much as 8 times in the smallest mass. Additionally, their research has shown that increasing the mass ratio increases the velocity amplification and is dependent on the coefficient of restitution.

In the very recent past, in the works of Kelly et al. [8], a velocity amplification machine has been manufactured and tested, validating the conclusions of the aforementioned research. The capabilities of this machine have produced repeatable acceleration ranging from 5,800 G to 23,400 G with durations of 28 to 44 microseconds, respectively. The machine is capable of testing microelectronics, such as MEMS components, within a frequency bandwidth up to 19 kHz.

In this paper, a commercially available dual mass impact amplifier (DMSA), based on similar velocity amplification theories as previously described, is investigated using transient finite element analysis. This DMSA can be attached to existing drop towers manufactured by the same company and is able to produce repeatable impact accelerations as high as 100,000 G. Through simulation, parametric insights are provided into the effect of DMSA design parameters on its performance.

The DMSA is found to produce an acceleration profile that is closer to the JEDEC half-sine standard [9], than does the velocity amplifier investigated by Kelly et al. [8], which produces a full sine wave, depending on the collision material. In the DMSA, the pulse is immediately damped and the reverse half pulse has less than 20% of the initial amplitude. As a result, failure data produced in board level testing on the DMSA can be more meaningfully compared with tests conducted as per JEDEC standards.

One of the goals of the transient finite element analysis (FEA) reported here is to be able to guide experimenters derive boundary conditions for local models of subsystems in the drop simulation, before actually conducting a drop test.

1.2.2 Simulation of board level drop tests with intentional board "slap" at high impact accelerations

The concept of acceleration magnification through secondary impacts is further exploited in Chapter 3 of this study to generate extremely high accelerations (>10,000 Gs) on printed wiring boards during drop testing. The secondary impact being explored here is between the test board and the mounting fixture. This impact can be used to amplify the acceleration produced on a drop tower or on a DMSA. Utilizing the principle of the DMSA and the velocity amplifier, the acceleration magnification can be maximized by allowing the test fixture to impact the PWA after the PWA has gained some significant deflection velocity.

Secondary impacts occur in practice due to clattering of portable electronic products after the initial drop, and have been investigated in papers by Shan et al. and Goyal et al. [10], [11], [12]. In these papers, a rod falling onto a hard surface at an angle was investigated as a simplified representation of an electronic product impacting a surface. The authors concluded that the bar could undergo a series of amplified velocity reversals orders of magnitude greater than in the initial drop and much higher than that prescribed in standardized tests.

Other than papers citing the aforementioned research, the literature is very limited regarding drop amplification on a PWB through secondary impact with its fixture. Askari et al. [2] concludes that there are definite indications that inner components and

impact each other at high accelerations in full product drop testing. Furthermore, acceleration responses are predicted with FEA and reputed to be unrealistic.

The purpose of this chapter is to investigate, though simulation, a clamped PWA impacting the fixture with different velocities. The impact velocity is varied by varying the clearance between the PWB and the fixture. The model uses an input-G method, where the boundary conditions were derived from high impact accelerations measured on the DMSA. The impact accelerations are measured at different locations on the board from the FEA output and compared to determine which separation distance produces the highest impact response [13]. The response of the PWB to initial drop is multi-modal and hence multiple natural modal frequencies and multiple mode shapes of the board contribute to the contact force at certain depths. This model was used to develop experimental guidelines to investigate the effect of fixture design on the drop durability of selected surface mount components:, in board level testing. Chapter 3 will show that "board slap" has a strong effect on the lifetime of the components mounted on the PWA.

1.2.3 Specimen design and failure analysis for board level drop tests with intentional board slap at high impact accelerations

Thorough research has been conducted on drop testing of wafer level chip scale packages (WLCSPs). The small dimensions and high I/O of WLCSPs have increased their use in portable electronic devices, as seen in Figure 1. As use of WLCSPs has become more common, the number of manufacturers has also increased as well, leading to increased diversity in different package structures in the market [14]. As a result, product reliability of different WLCSP packages must be investigated. In works by Chen et al. [15], SAC105 was preferred in board level testing. Solders with higher silver

content had a shorter failure lifetime in board level testing [9] at 1500 G with a 1.0 ms pulse duration. Pasi et al. [14] had similar results in smaller WLCSP packages. In numerous papers reviewed on reliability of WLCSPs in dynamic loads (including high rate four point bend tests), failures were in solder interconnects, in the intermetallic (IMC) layer on the component side. Furthermore, the failure site was in the corner ball [14], [15], [16]. Alajoki et al. [16] concludes that IMC failures at the corner balls on the component side are due to three factors: higher normal stresses, brittleness of the reaction layer(s), and the strain-rate hardening of the bulk solder interconnections. Only one paper reviewed, Xueren et al. [17], found failures at the Cu trace under the corner ball as the most common failure site. This is most likely due to poor board design (trace dimensions, sharp angles, etc.) and construction.

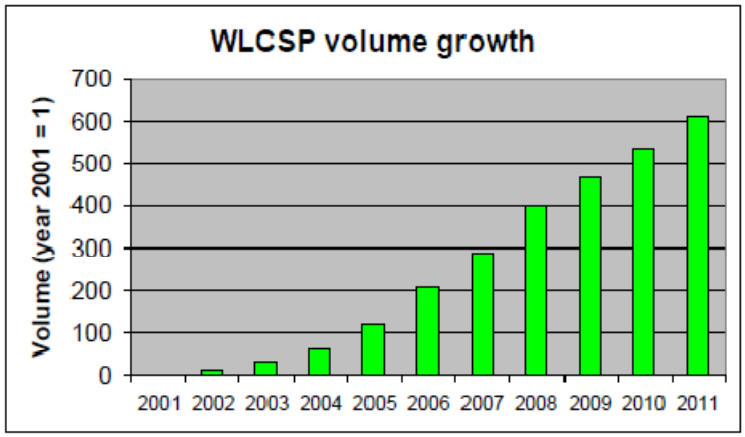

Figure 1: Rough estimation of WLCSP growth in volume [14]

Micro Electro Mechanical Systems (MEMS) are also becoming increasingly popular in portable devices. These components can be found in products ranging from cell phones to missiles because of the multitude of structures that can be manufactured (RF switches, accelerometers, gyros, microphones, etc.). Due to their popularity in many aerospace, and other industrial applications, these products can be subjected to extremely

harsh conditions. For example, launch vehicles have resonant frequencies around 50 Hz, requiring these structures to be designed with natural frequencies far outside of this range [18]. In a paper by Sheehy et al. [19], these products required accelerations as high as 40,000 G to induce failures. The main failure mechanisms differ in every structure and load condition, but typically under impact loads structures are susceptible to brittle fracture.

In chapter 4 of this thesis, durability under repeated secondary impacts is discussed. As previously mentioned, two different components, WLSCP49s and COTS (commercial-off-the-shelf) MEMS microphones were drop tested at high accelerations ranging from 10,000 G to 30,000G.

The WLCSP49 board described in the chapter, had a significantly lower lifetime under secondary impact with the fixture, compared to a freely deflecting board. Moreover, the WLCSP49 failure mechanisms matched tests at JEDEC standards (1,500 G and 2,900 G). The same was seen in MEMS testing with intentional secondary impact between the test PWB and the fixture.

1.3 Thesis layout

The thesis is divided into different chapters, each building on the previous. In chapter 2, a detailed description of the test setup will be discussed, including the drop tower, and DMSA. It will also introduce FEA of the drop tower system (including the DMSA) and analytical models of secondary impact. Chapter 3 will introduce a generic description of the drop test specimen and test fixture. FEA of the impact between the test PWA and its fixture will be provided. In chapter 4, a case study of two different component types with different fixture types, one involving board slap, will be discussed. Finally, in Chapter 5,

general conclusions of the entire thesis will be provided and intellectual contributions will be highlighted. Limitations of the current work will be discussed and future work will be recommended.

2 Simulation of secondary impact to generate very high accelerations

2.1 Introduction and problem statement

Since the introduction of popular portable products like smart phones, GPS units, and Net books, industry leaders in consumer based electronics have been shifting their focus to impact and drop characterization of portable devices. Recently, there has been increasing interest in conducting lifetime testing at high accelerations as high as 30,000 G. Industry impact qualifications for board level testing commonly follows guidelines and methods set by JEDEC [9], but these standards limit the acceleration to lower levels (<5,000 G). However, consumer feedback reveals that dropping electronics onto a hard surface can induce very high acceleration or deceleration, ranging from 10^4– 10^5 Gs [20]. Furthermore, in aerospace and weapons systems, electronics are often exposed to extremely high accelerations during launch.

Thus, the need for creating a test apparatus to provide repeatable testing of electronic assemblies at a full spectrum of accelerations becomes of paramount importance [8]. Drop tower manufacturers offer a dual mass impact amplifier (DMSA) device as a means to achieve very high accelerations (10^4 – 10^5 Gs). Commercial drop tower systems are designed for repeatable testing up to high drop counts, at acceleration levels typical of JEDEC standards. The drop tower seen in Figure 2 is capable of reaching impact accelerations as high as 5,000 G. The bare drop tower consists of a drop table,

seismic base, and pulse shaping material. The drop table falls, along the guide rods, from a given height onto the seismic base. The pulse shaper, also called a pulse programmer, sits on the seismic base and determines the magnitude and duration of the impact. The seismic base is fitted with pneumatic pistons to cushion the impact onto the floor of the lab and has little effect on the acceleration response.

As previously mentioned, the commercial DMSA accessory can amplify this impact acceleration range by up to 20x. The DMSA consists of a base and a suspended mass. In a drop test the suspended mass moves along the guide rods against the force of the springs and impacts the base. There is a pulse shaper sheet located in between the DMSA base and the DMSA table. The purpose of the springs is to prevent multiple impacts. The base of the DMSA, as seen in Figure 3, is fixed to the drop table of the drop tower, and like the drop tower, can produce repeatable impact accelerations. These accelerations are generated in the DMSA by the collision of two significantly different masses, as seen in Figure 3, traveling at opposite velocities. The DMSA on the drop tower system can be seen in Figure 2 on the right. The DMSA and drop table fall from a height onto the seismic base. An elastomeric cylinder (Delrin in this study) fixed to the seismic base acts as a pulse shaper and influences the magnitude and duration of the drop table and DMSA base. The elastomer cylinder was chosen as the pulse shaping material because of its compliance and thus its ability to produce very long duration acceleration pulses of relatively low amplitude, as seen in Figure 4. The drop table (and DMSA base) rebound off of the elastomer pulse shaper and impact the falling DMSA table. A thin paper sheet was chosen as the pulse shaping material in between the DMSA base and table because it smoothed out the high frequency ringing produced in metal to metal

impact; yet it did not significantly reduce the magnitude or increase the duration of the impact. The low magnitude and long duration response of the drop table (and the DMSA base) and the high magnitude, short duration acceleration response of the DMSA table can be seen in Figure 4. In this figure the DMSA table amplifies the peak acceleration of the drop table by approximately 18x. A more detailed understanding of the physics of the drop tower will be provided in Section 2.2.1.

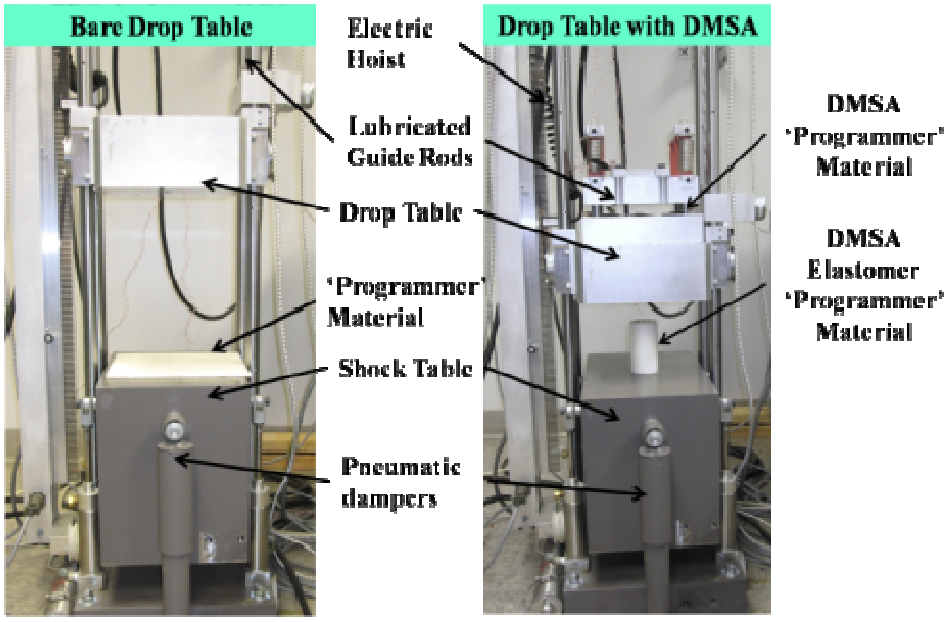

Figure 2: Commercial drop tower with details marked.

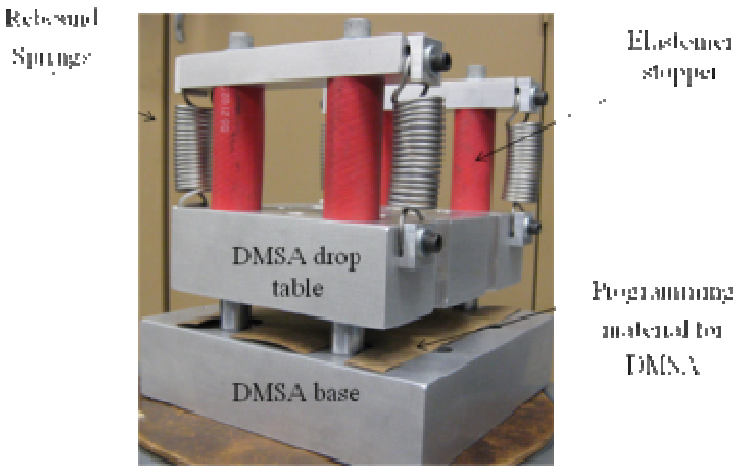

Figure 3: Dual mass impact amplifier (DMSA) with details marked.

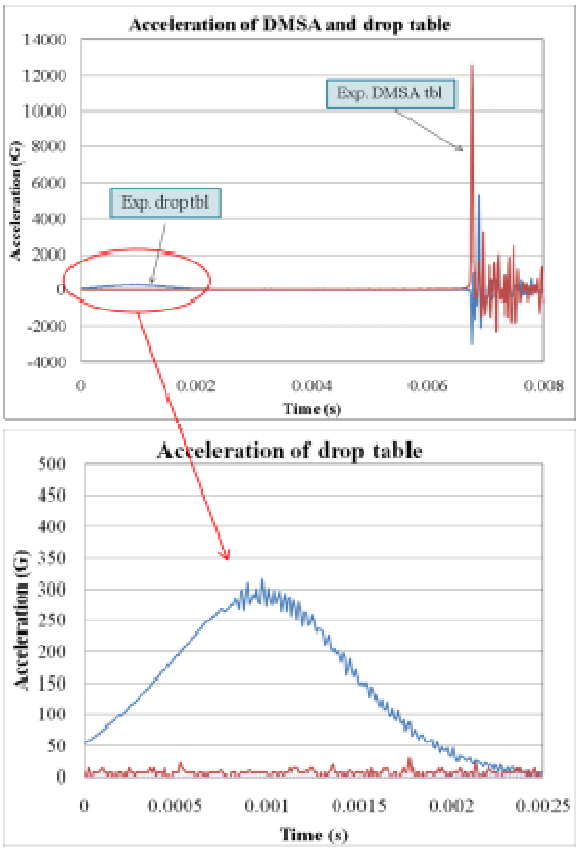

Figure 4: Acceleration profiles of the drop table and DMSA table in a secondary impact test.

2.2 Approach and parametric studies

In this section, the drop tower will be described starting with very simple analytical models and finishing with a complex FEA simulation. The purpose of this

section is to find and exploit different parameters (structural, interaction, etc.) to determine the influence on the DMSA table acceleration response.

2.2.1 Simple analytic model of velocity impact of the drop table and DMSA assembly

In this section, spring-mass models are used to describe the acceleration response of the drop and DMSA tables. The amplitudes of these responses can be compared to show that the DMSA table amplifies the peak acceleration of the drop table.

2.2.1.1 Simplified primary impact

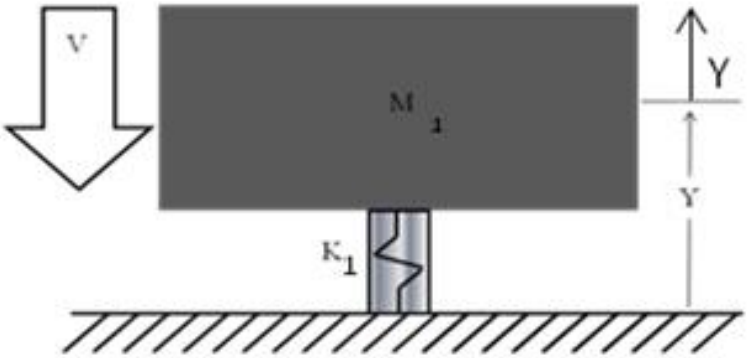

Figure 5: Single DOF description of the initial impact between the drop table (with the DMSA base), M_1, and the impact table, separated by an elastomer pulse shaper, K_1.

The drop tower, without the DMSA accessory, can be modeled as a single degree-of-freedom (DOF) system with a spring and damper when the drop table is in contact with the elastomer pulse shaper. To simplify this problem even further the effects of damping have been excluded as seen in Figure 5. Similar dynamic analysis and simulations was presented by E.H. Wong et al. to describe the dynamics of a fixed PWB during a drop test [21]. The equations of motion for a single DOF model can be found in most textbooks and solved quite easily. The following equations can be used to derive the amplification, or the response acceleration half sine amplitude, as a function of the drop height, stiffness, and mass of the drop table.

Assuming the initial conditions Y(0) = A and v(0) = v_o, the solution can be derived as follows. Force equilibrium leads to the equation:

$$M_1\ddot{Y}_1 + K_1Y_1 = 0 \tag{2.1}$$

Assuming a harmonic solution, this second order ordinary differential equation can be solved for the natural frequency of the system,

$$\Omega^2 = \frac{K_1}{M_1} \tag{2.2}$$

$$Y(t) = Asin(\Omega t) \tag{2.3}$$

Using the initial conditions given above, this leads to the following harmonic motion:

$$Y(t) = Asin(\Omega t) = \frac{v_o}{\Omega}\sin(\Omega t) \tag{2.4}$$

$$Y(t) = Asin(\Omega t) = \frac{v_o}{\Omega}\sin(\Omega t) \tag{2.5}$$

$$\ddot{Y}(t) = -v_o\Omega\sin(\Omega t) = A_o\sin(\Omega t) \tag{2.6}$$

The amplitude of the acceleration, A_o, and the duration of impact, t_o, can be derived in terms of the mass of the table M_1, the stiffness of the elastomer K_1, and the drop height h.

$$A_o = \sqrt{\frac{2ghK_1}{M_1}}, \quad t_o = \pi\sqrt{\frac{M_1}{K_1}} \tag{2.7}$$

2.2.1.2 Simplified secondary impact

The DMSA generates high impact accelerations through secondary impact. After the first impact between the drop and impact tables, the drop table (and the DMSA base) rebounds and the DMSA suspended mass and the drop table (with the DMSA base), start to travel with opposing velocities and collide. Solving the equations of motion for a two DOF mass spring system, again excluding damping for simplicity, can qualitatively show the amplification of the initial primary impact due to the secondary impact. The two DOF model can be seen in Figure 6. Guided by detailed finite element simulations (reported in Section 2.2.4) the gravitational force is assumed to be trivial in comparison to the impact forces. Using the initial conditions at the time of impact between these masses, the acceleration amplitude is derived in terms of the height of the drop, the stiffness of the elastomer**,** stiffness of the paper pulse shaper between the masses, and the mass of the tables [22].

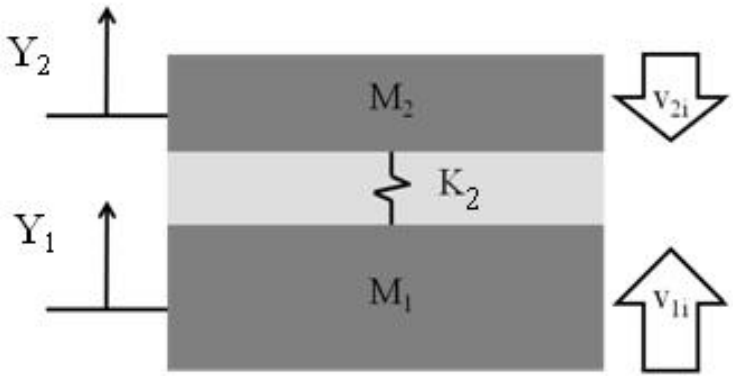

Figure 6: Two DOF model representing the collision of the DMSA table (M_2) and the drop table with the DMSA base (M1), separated by an elastomer sheet of stiffness, K_2

$$M_1\ddot{Y}_1 + K_2(Y_1 - Y_2) = 0 \tag{2.8}$$

$$M_2\ddot{Y}_2 + K_2(Y_2 - Y_1) = 0 \tag{2.9}$$

Assuming the motion is periodic and harmonic:

$$Y_1 = Asin(\omega t + \emptyset) \quad 2.10$$

$$Y_2 = Bsin(\omega t + \emptyset) \quad 2.11$$

$$\ddot{Y}_1 = -A\omega^2 sin(\omega t + \emptyset) \quad 2.12$$

$$\ddot{Y}_2 = -B\omega^2 sin(\omega t + \emptyset) \quad 2.13$$

Solving for the natural frequencies by using the assumed motion, the first natural frequency is zero and represents rigid motion of this free-free system.

$$\omega_1 = 0,\ \omega_2 = \sqrt{\frac{K_2(M_1 + M_2)}{M_1 M_2}} \quad 2.14$$

Using the initial conditions $Y(t_i) = Y_o$ and $v(t_i) = v_o$, the solution constants can be determined.

$$A = \sqrt{{Y_{1i}}^2 + \left(\frac{v_{1i}}{\omega}\right)^2}, B = \sqrt{{Y_{2i}}^2 + \left(\frac{v_{2i}}{\omega}\right)^2} \quad 2.15$$

If the tables are idealized as rigid masses, the equation can be simplified even further when we compare the impact amplitudes in Equations 2.7 and 2.17.

$$v_{2i} \approx \sqrt{2gh} \quad 2.16$$

$$A_1 = -B\omega^2 = \frac{v_{2i}}{\omega}\omega^2 = v_{2i}\omega \quad 2.17$$

$$\frac{A_1}{A_o} = \frac{v_{2i}\sqrt{\frac{K_2(M_1+M_2)}{M_1M_2}}}{\sqrt{\frac{2ghK_1}{M_1}}} = \frac{v_{2i}\sqrt{\frac{K_2(M_1+M_2)}{M_1M_2}}}{v_{1i}\sqrt{\frac{K_1}{M_1}}} = \sqrt{\frac{K_2}{K_1}\frac{M_1}{M_2}+\frac{K_2}{K_1}} \qquad 2.18$$

Assuming the pulse shaper between the tables is very thin, the stiffness K_2 for the second impact between the aluminum DMSA and drop table is greater than K_1 for the first impact between the drop table and the elastomer cylinder. Similarly, the mass of the DMSA table is generally much smaller than the combined mass of the drop table and the DMSA base. Thus

$$\frac{K_2}{K_1} > 1 \; upper \frac{M_1}{M_2} \approx 8 \qquad 2.19$$

Using these assumptions, comparison of the amplitudes shows that the acceleration due to the initial impact is amplified by the second impact between the two masses. Approximations of the mass ratio, 8, and the stiffness ratio, 10, can provide insight to a possible amplification factor. Thus:

$$\frac{A_1}{A_o} \gg 1 \approx 9 \qquad 2.20$$

The motion and velocity of the drop tower is modeled below as a function of time using simple kinetics of momentum conservation between two rigid bodies. This model does not include the impact dynamics described in Equations 2.1 - 2.20, or the strain energy of the impacting masses and the DMSA springs, or non-conservative external forces such as guide-rod friction. However, these plots can be used for simple first order insight into the system dynamics. The displacement plot in Figure 7 depicts the relative

motion between the DMSA table and the drop table with the DMSA base. The inputs to this model are simply the drop height, h = 1 m, the masses of the DMSA table, M_2 = 10 kg, and drop table with DMSA base, M_1 = 80 kg, and the clearance between the tables, d = 0.21 m. The velocity plot in Figure 8 shows the initial and final velocities after the initial impact between the drop table (with the DMSA base) and the pulse shaper (elastomer cylinder), and the secondary impact between the DMSA table and the drop table (including the DMSA base).

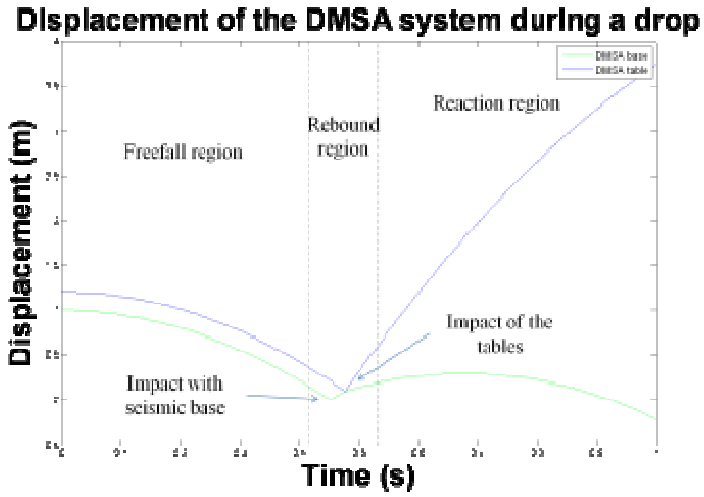

Figure 7: Displacement of the drop tower with the DMSA accessory during a drop test.

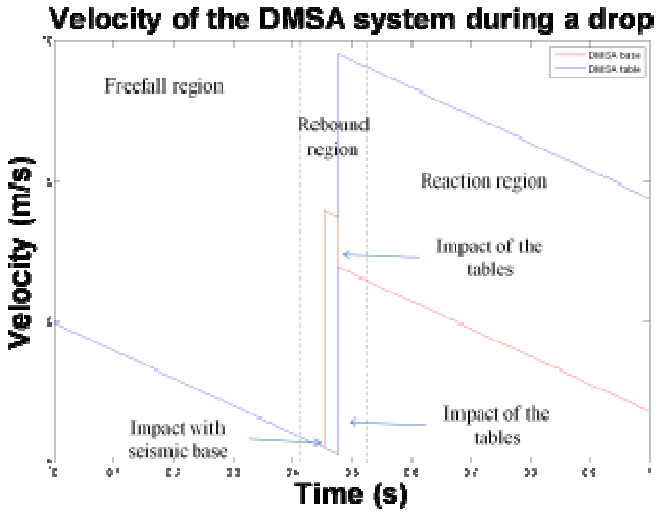

Figure 8: Velocity of the drop tower with the DMSA accessory during a drop test.

2.2.2 Detailed computational modeling methods

To obtain more detailed insights into the effect of the impact dynamics on the acceleration history, the drop tower and DMSA system were modeled with commercial finite element simulation software [23]. The model inputs include table dimensions, manufacturer's spring constants, and pulse shaper material properties. as seen in

Table 1. These parts are labeled in Figure 9. Acceleration time histories were captured at rigid points of the DMSA and drop table and used as input loading boundary conditions for this model. Studies were conducted to understand the effect of the contact modeling methods and the contact model parameters on the predicted results, as explained below in Section 2.2.3.

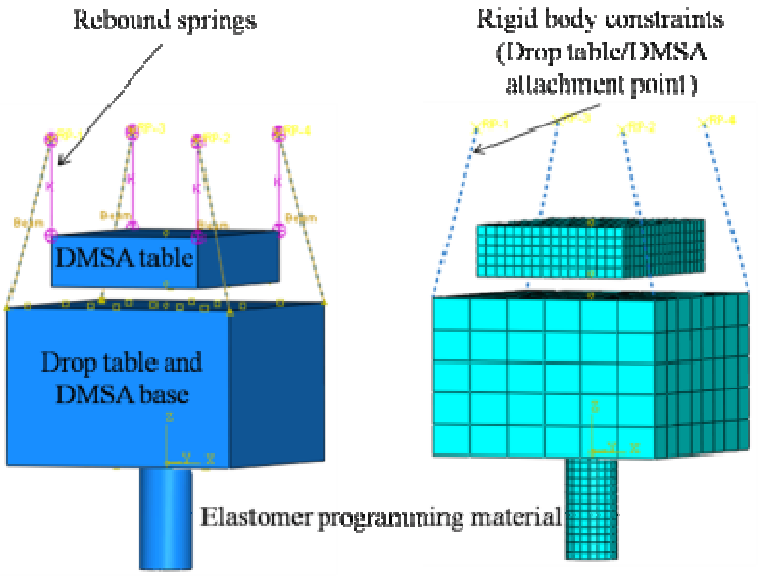

Figure 9: Drop tower assembly velocity model with DMSA and elastomer pulse shaping material.

Table 1: Model structural parameters

Model Parameters	
DMSA spring stiffness	1200 N/m
DMSA table dimensions	0.197 m x 0.152 m x 0.049 m (L x W x H)
DMSA base and drop table dimensions	0.23 m x 0.23 m x 0.15 m (L x W x H)
Elastomer cylinder pulse shaper	0.101 m x 0.0508 m (height x diameter)

2.2.3 Model of contact dynamics

In this section, dynamic interactions in the FEA model are explored. Definitions of different contact types are summarized and implemented in simple FEA models to compare effects on the acceleration response. Damping parameters are also investigated.

2.2.3.1 Definitions

There are two ways to define contact in the FEA software used in this study: penalty method and kinematic contact method. They are used for defining the impact between the DMSA and drop tables as well as between the drop table and the elastomer cylinder pulse shaper. There are fundamental differences between these two modeling approaches. The penalty method approximately enforces the contact constraints using weight functions that represent contact stiffness, while the kinematic method exactly enforces the constraint condition through a predictor corrector algorithm. In other words, the penalty method always allows for some penetration of the nodes of the slave body into the master body, but any penetration occurring in the kinematic method is corrected with the algorithm.

The kinematic contact method can only be used to model a hard contact in this explicit dynamic FEA code and contact damping is not allowed. The depth of interpenetration of the slave node into the master surface, the mass assigned to the slave node, and the time increment are used to calculate the resisting force required to prevent penetration [23]. This method was ideal for simulating the primary contact between the drop table and the elastomer pulse shaper cylinder since the compliance of this contact is already captured by explicitly modeling the deformation of the elastomer pulse shaper cylinder. Thus the material properties of the elastomer cylinder pulse shaper account for the amplitude and duration of the reaction force. Compared to the penalty method, the accuracy of the kinematic method is less sensitive to the length of the time step and thus provides a faster analysis.

In explicit dynamic FEA, penalty contact can be defined as hard or soft. Penalty method, hard contact minimizes node interpenetration and does not allow transfer of tensile stress across the surface, creating higher reaction forces during impact. In softcontact the contact pressure is allowed to linearly increase as a function of the clearance as the two contacting surfaces approach and interpenetrate each other. In soft contact the amplitude of the reaction force is decreased and duration of the force is increased due to greater node interpenetration. The penalty method with soft contact is suitable for mimicking a thin interfacial attenuation layer on the surface of the master mesh [23]. In regards to the actual test setup, this was used to implicitly account for the presence of the thin cardboard pulse shaper sheet between the DMSA table and the DMSA base/drop table when modeling the secondary impact. The downside of the penalty method is its computational requirement. The accuracy of individual solution

iteration depends on the length of the time step and the penalty method can shorten the critical stable time step, thus increasing the computation time.

2.2.3.2 Simplified models

Simple finite element models were created to explore the different definitions of contact and to investigate the effect of different contact parameters. The simple models reduced computational time and provided immediate results for analysis as seen in Figure 10. Contact stiffness was parametrically varied to find a value that imitated the behavior of the pulse shaper sheet used experimentally. Further studies were conducted to investigate the effects of contact damping. These results, as explained in greater detail below, were used to tailor the DMSA/drop tower model to better represent the dynamics of the experimental system. A simple analytic model of contact damping in a single degree-of-freedom system was also developed to verify the trends predicted by the simple FEA model.

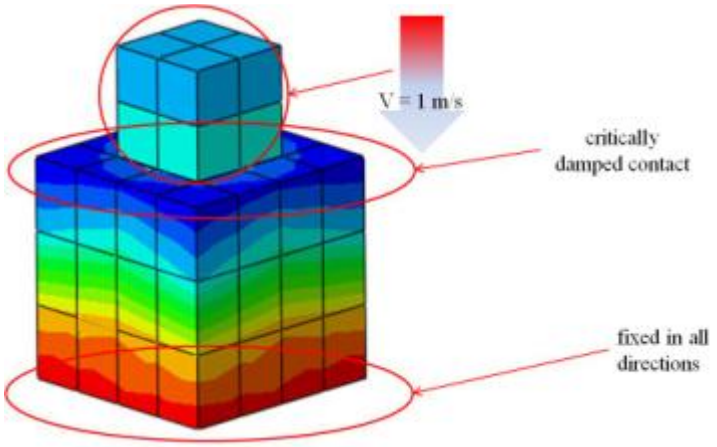

Figure 10: Simple model FEA used to investigate contact stiffness and damping factors.

2.2.3.2.1 Critical damping

In the explicit dynamic FEA analysis, contact damping is not available for the hard kinematic contact model. However, penalty contact method has a default critical damping

fraction of 0.03, which can be modified by the user. As seen in Section 2.2.1.2, the pulse shaper sheets between the DMSA and drop tables can be modeled as a spring and damper system while the masses are in contact. Therefore, contact damping was parametrically studied: first in the simple model FEA simulations and then in the full assembly model. The numerical values of the mass, drop height, velocities of the masses, and the stiffness in the simple models were not significant, but provided qualitative insight into ways to best model the system in subsequent detailed studies.

The charts below show the different parametric studies conducted on the full assembly model to investigate the effects of contact damping. The solution from FEA simulations, as seen in Figure 1 shows that the peak acceleration passes through minima at a critical damping fraction of approximately 0.07.

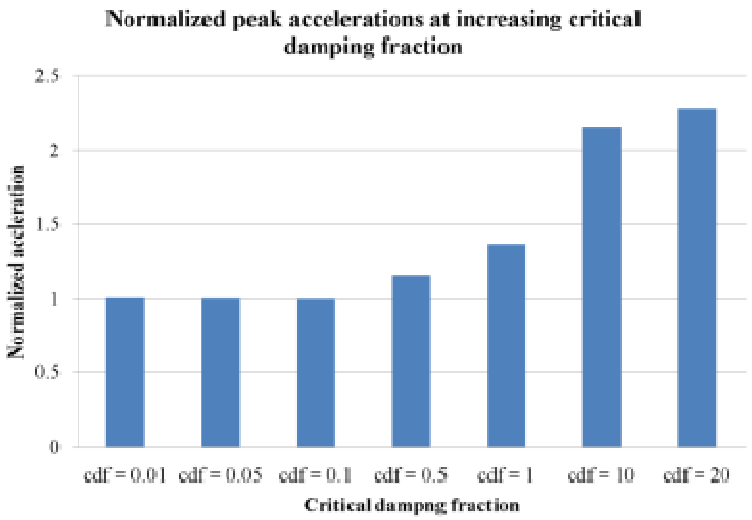

Figure 11: Acceleration analysis of the critical damping fraction.

The presence of this minima can also be analytically confirmed with a single degree of freedom spring mass damper system similar to Figure 5. Excluding the force of gravity and including the initial conditions Y_o and v_o, the equations of motion become:

The characteristic equation can be written seen in Equation 2.22, where ξ is the critical damping fraction.

$$\ddot{Y}_1 + 2\xi\omega_n\dot{Y}_1 + \omega_n^2 Y_1 = 0 \qquad 2.22$$

The general solution of this second order differential equation is given as,

$$Y_1(t) = C_1 e^{s_1 t} + C_2 e^{s_2 t} \qquad 2.23$$

Where $Y_1(0) = C_1 + C_2 = Y_{10}$ and $\dot{Y}(0) = s_1 C_1 + s_2 C_2 = v_0$.

$$C_1 = \frac{-s_2 Y_{10} + v_0}{s_1 - s_2} \qquad 2.24$$

$$C_2 = \frac{s_1 Y_{10} - v_0}{s_1 - s_2} \qquad 2.25$$

Using these values in the general solution in equation 2.23,

$$Y(t) = \frac{-s_2 Y_{10} + v_0}{s_1 - s_2} e^{s_1 t} + \frac{s_1 Y_{10} - v_0}{s_1 - s_2} e^{s_2 t} \qquad 2.26$$

The roots of the characteristic equation for an underdamped system $0 < \zeta < 1$ can be seen in Equation 2.27, where $\omega_d = \sqrt{1 - \zeta^2}\omega_n$

$$\begin{matrix} s_1 \\ s_2 \end{matrix} = -\zeta w_n \mp i w_d \qquad 2.27$$

Simplification of the $Y_1(t)$ term leads to the solution as a function of ξ and the initial conditions seen in equation 2.28.

$$Y_1(t) = \sqrt{{Y_{10}}^2 + \left(\frac{\xi w_n Y_{10} + v_0}{w_d}\right)} e^{-\xi w_n t} \cos\left(w_d d - tan^{-1}\frac{\xi w_n Y_{10} + v_0}{w_d Y_{10}}\right) \qquad 2.28$$

Differentiating this equation twice with respect to time will give the acceleration response of the single DOF system. The acceleration response derived from Equation 2.28 is plotted as a function of the critical damping fraction, as seen in Figure 12. This plot has a minimum, and confirms the validity of the FEA results seen earlier in Figure 11.

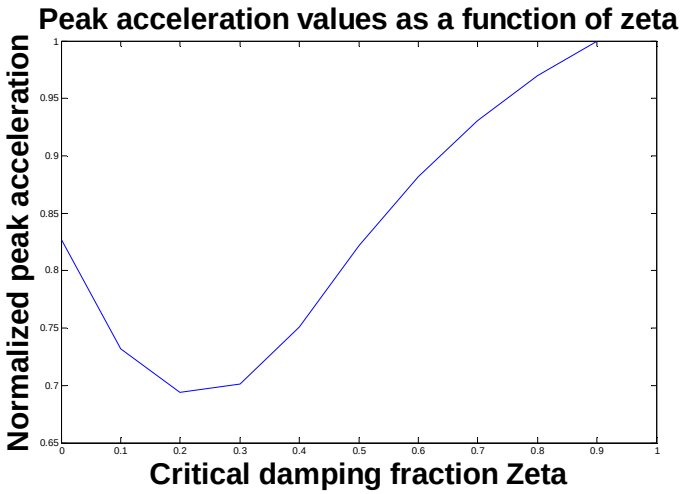

Figure 12: Peak acceleration values as a function of the critical damping fraction derived from the single DOF model.

Figure 13 shows the comparison between experimental measurement and FEA parametric simulations run with different contact damping and contact stiffness values, as labeled in the Figure 13. The DMSA response is clearly dependent on the contact damping and stiffness. Analysis shows that with the minimum contact damping and appropriate contact stiffness, the DMSA experimental response can be predicted within 15%.

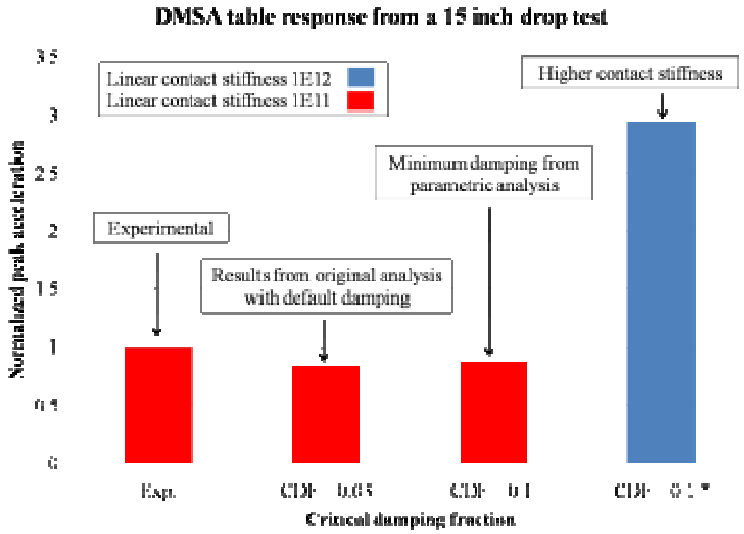

Figure 13: Combined contact parameters.

2.2.3.2.2 Material damping

Rayleigh damping is used for modeling selected materials in the FEA simulation. These parameters can be seen in the damping matrix [C] in Equation 2.29 where α is the mass-proportional damping and β is the stiffness-proportional damping coefficient, respectively. The mass proportional damping coefficient, α, dissipates lower frequency modes by introducing forces caused by the absolute velocities of model. The stiffness proportional damping coefficient, β, dissipates the higher frequency modes. The β coefficient is actually defined as viscous material damping, which creates additional damping stress proportional to the strain rate and current elastic stiffness. The additional damping stress is not included in the simulation output and is only used to converge the solution when the β coefficient is defined in the material.

2.29

Changes in the Rayleigh damping parameters of the elastomer cylinder pulse shaper material had minimal effect on the acceleration responses of the DMSA table and drop table. In both cases, the effect of changing α damping parameter was less than 0.1%, as

seen in Figure 14. Interestingly, there is a non monotonic trend in the acceleration of the DMSA table, as a function of pulse shaper damping value, as seen in Figure 15. The maximum response occurs α=0.3. The β damping parameter caused the simulation to run longer and when used in the simple contact models, gave infeasible acceleration response output. Therefore, it was not used in the full assembly model of the drop table and DMSA. Overall, Rayleigh damping of the elastomer pulse shaper cylinder had little or unwanted effects on the acceleration response during impact. Table 2 shows the contact parameters used in the initial conditions model described in the next section.

Table 2: Initial conditions model contact properties

Contact Properties			
	Type	**Stiffness**	**Damping**
DMSA pulse shaper	Penalty	1.00E+11	0.1
Drop table pulse shaper	Kinematic	Hard (N/A)	N/A

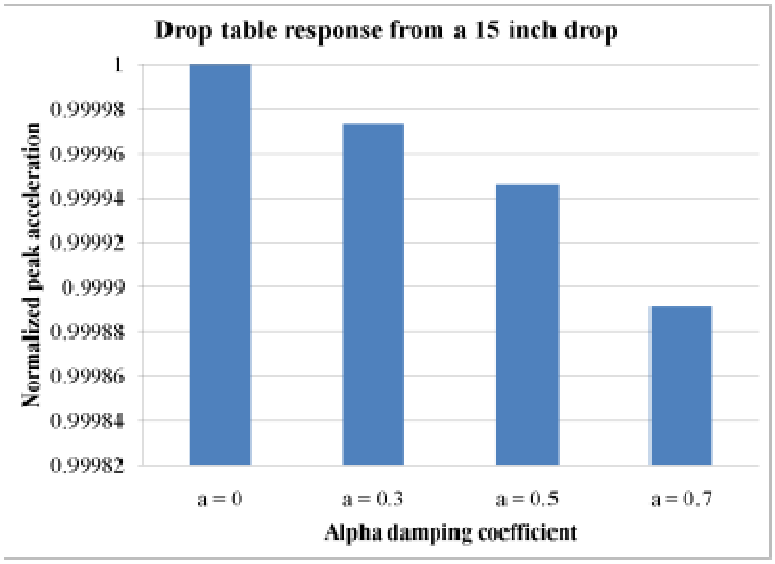

Figure 14: The effect of mass proportional damping defined in the elastomer material on the initial impact of the drop table with the DMSA base.

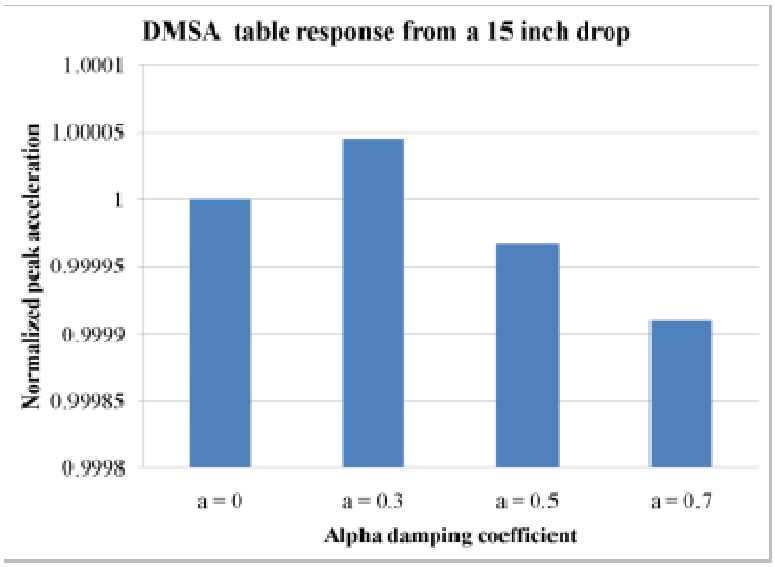

Figure 15: The effect of mass proportional damping defined in the elastomer material on the second impact between the DMSA table and drop table with the DMSA base.

2.2.4 Overview of initial condition method in model

As previously mentioned, the full assembly (the drop tower with DMSA accessory and pulse shapers), was modeled in FEA software. Simulations were conducted by applying the velocity just before impact, derived from the drop height, to the moving features. The acceleration-time response of the independently moving rigid body features was investigated and parametrically studied. The model includes structural and pulse shaping material properties**,** as seen in Table 3 [13] . Figure 16 and Figure 17 is a comparison of the response of the DMSA in the experiment using high speed video and screen shots of the response of the drop table and DMSA in the simulations.

Table 3: Model material properties

Material Properties			
	E (Pa)	**ν**	**ρ (Kg/m^3)**
DMSA and drop tables	7.0E10	0.3	2700
Elastomer	3.0E9	0.33	1500

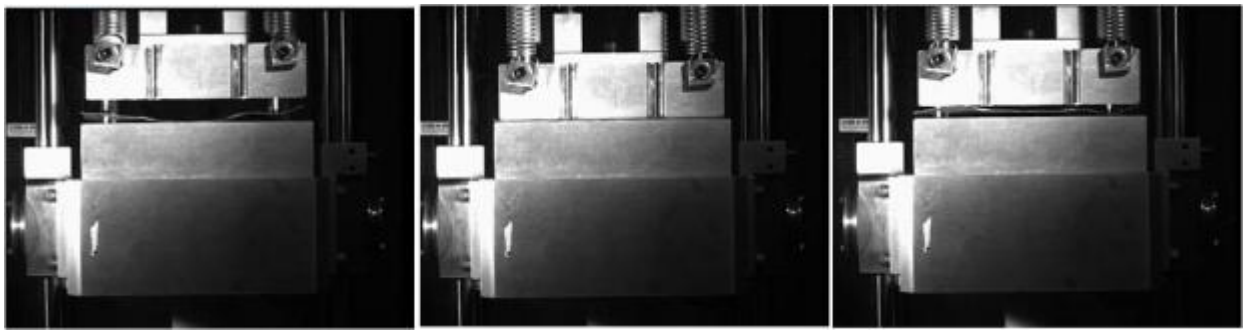

Figure 16: High speed video capture of the drop table with the DMSA accessory. Left to right chronologically, after the initial impact, second impact of the DMSA table and the drop table with the DMSA base, after the secondary impact.

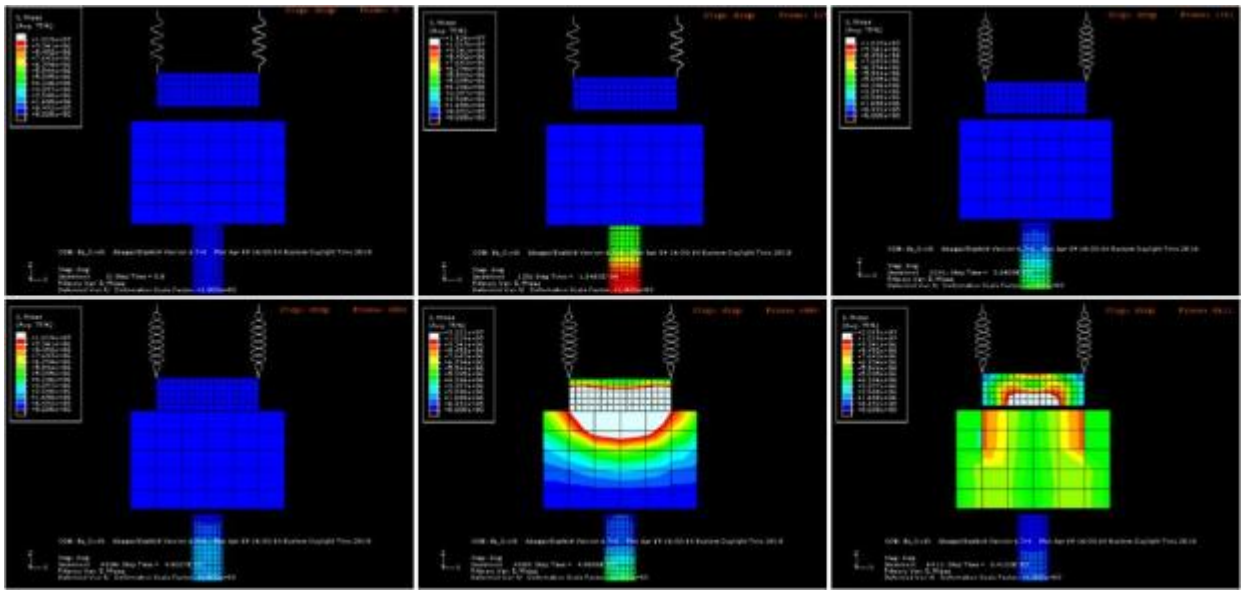

Figure 17: Drop tower with the DMSA accesory FEA simulation screen shots. Left to right, top to bottom chronologically: Just before the initial impact with the elastomer, during impact with the elastomer, after the secondary impact between the tables.

In this model, external non-conservative forces were excluded and other simplifications were used. The model constrains the drop table to move only in the vertical direction to imitate guide rods. In the real assembly the DMSA is mounted to the drop tower with 4 corner bolts. In the model the DMSA base and the drop table mass are combined and the dynamic interactions are excluded. The base of the elastomer pulse shaper is fixed in all six degree-of-freedom (DOF) to represent a flat rigid connection to the surface of the seismic base (not shown in the model). Including the seismic base, the

effects of pneumatic dampers connected to the seismic base were not included. Since the guide rods were not physically modeled, small rotations caused by friction between the table coupling and the guide rods was excluded.

The model has been validated as shown in Figure 18. The model output is shown compared to the experimental output for a 15 inch drop from the drop tower with the DMSA accessory. There is some discrepancy, 2 ms, between the model prediction and experimental measurement of time to impact of the DMSA table (secondary impact). In the experiment, the time difference between the primary impact, between the drop table and the elastomer cylindrical pulse shaper rod, and the secondary impact, of the two masses, is approximately 6 ms. The model under predicts this value by approximately 2 ms. This is possibly because of the drag through contact friction from the drop table sliders coupled to the guide rods. The effect of gravitational forces was investigated and found to be trivial. This divergence can also be seen in the table velocities in Figure 19 . Notably, the peak acceleration is 2,000 G less than the experiment and the pulse width is wider. This disparity is related to the contact stiffness defined in the interactions between the tables.

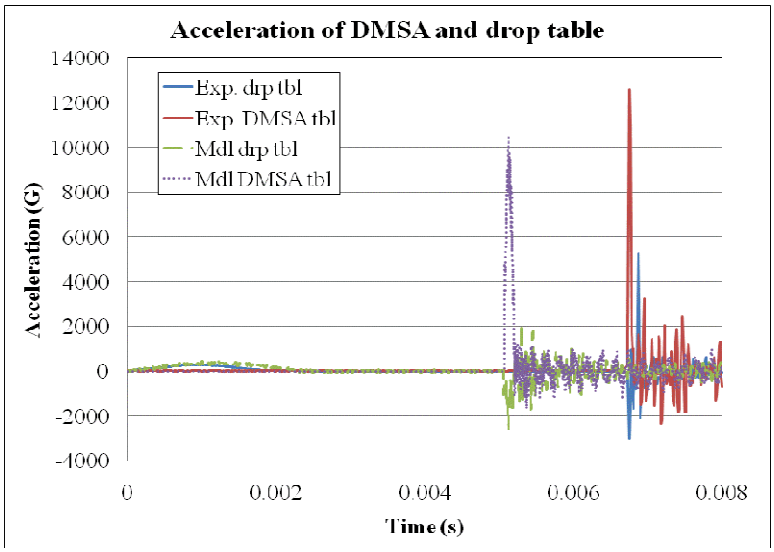

Figure 18: FEA vs experimental acceleration during a 15 inch drop.

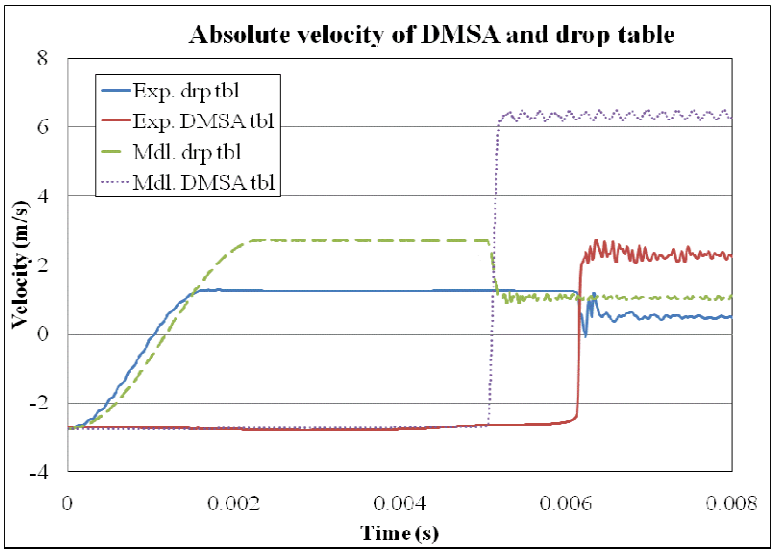

Figure 19: FEA vs experimental velocity during a 15 inch drop.

2.2.4.1 Parametric studies

Structural dimensions and materials properties parametrically varied for DMSA optimization are (i) drop table mass, (ii) rebound spring constants, and (iii) clearance between the DMSA table and DMSA base. These studies investigated the acceleration-time response during impact.

2.2.4.1.1 Drop table mass

The model was modified to study the acceleration-time with changing mass of the DMSA table. The density and table dimensions were used to back out the mass of the table and then the density of the material was redefined in each simulation to imitate added mass. The added mass could replicate a fixture being added to the table. The peak accelerations, derived from the acceleration-time response, showed a steady decrease as mass was added to the table as seen in Figure 20.

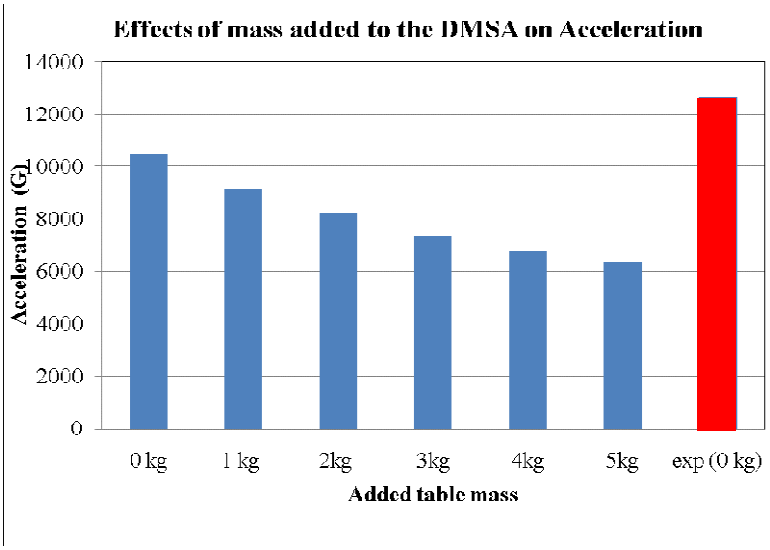

Figure 20: Peak acceleration values from the DMSA table with added mass during a 15 inch drop.

Simple conservation of momentum equations for an elastic collision show this response qualitatively. Note that v_{1i} and v_{2i} are of opposite signs when the two masses collide.

$$\rho_i = \rho_f \tag{2.30}$$

$$m_1 v_{1i} + m_2 v_{2i} = m_1 v_{1f} + m_2 v_{2f} \tag{2.31}$$

$$CR = \frac{v_{2f} - v_{1f}}{v_{1i} - v_{2i}} \tag{2.32}$$

$$m_1 v_{1i} + m_2 v_{2i} = m_2 v_{2f} - m_1[CR(v_{1i} - v_{2i})i v_{2f}] \tag{2.33}$$

$$\frac{m_1 v_{1i} + m_2 v_{2i} + m_1[CR(v_{1i} - v_{2i})]}{m_1 + m_2} = v_{2f} \tag{2.34}$$

Plotting the velocity-mass response of these masses we see a decrease in velocity of the table as m_2, the DMSA table mass is increased. This can be seen normalized in Figure 21.

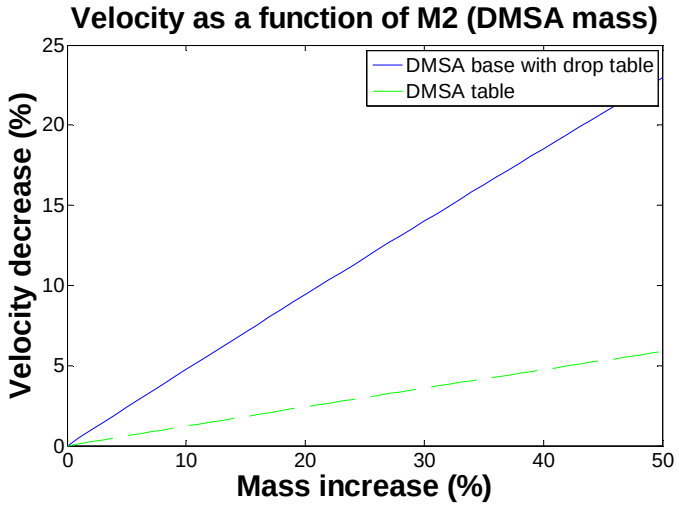

Figure 21: Final velocity of the tables after the second impact, as the DMSA table mass is increased.

2.2.4.1.2 Rebound springs

The rebound springs prevent the DMSA table from clattering against the DMSA base and to prevent double impacts during a drop. The springs are located at the four corners of the DMSA model and slightly offset from the corners in the experiment. The springs had little effect on the displacement, velocity, and acceleration-time histories;

however, there is a shallow downward trend, as expected, in the peak response values. These values are trivial and are not worth investigation.

2.2.4.1.3 Clearance between the DMSA table and drop table

As mentioned in section 2.2.4, the impact of the two tables occurs earlier in the simulation when compared with the first impact of the drop table and the elastomeric cylindrical pulse shaper. Increasing the distance between the DMSA and the DMSA base can significantly decrease the time to impact as seen in Figure 22. A slight decrease in the peak acceleration values was also observed in the simulation as the clearance was increased. The decrease in peak acceleration values could be from the influence of gravity on the initial velocity and computational variation from numerical round off in explicit analysis.

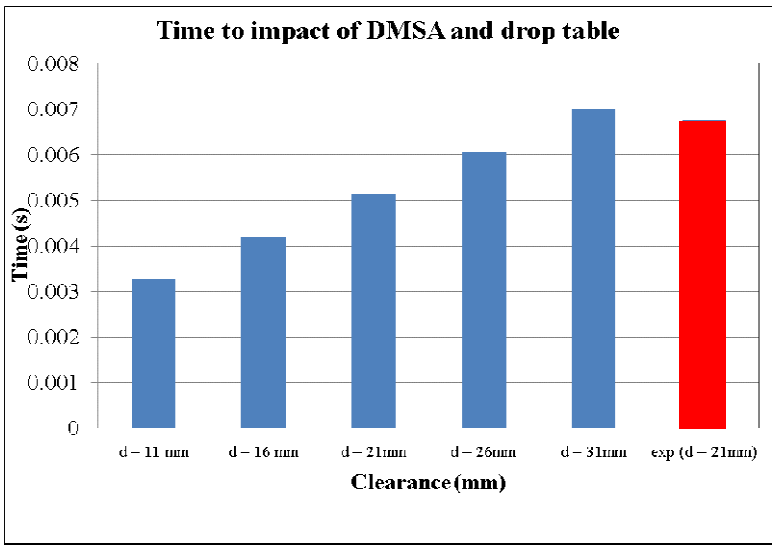

Figure 22: Time to impact of DMSA and drop table.

2.2.4.2 Conclusions from Initial Conditions model:

The simulation and experiment have good agreement in the acceleration and velocity-time histories. The peak acceleration values can be manipulated by adjusting the contact parameters to match the experiment. The initial impact matched well and can be

changed by redefining the material properties of the elastomer. The second impact acceleration pulse magnitude and the width are caused by the magnitude of the user defined contact penalty stiffness and contact damping. External forces, drag from friction from the table coupling to the guide rods, are believed to cause the time delay of the second impact.

The simulation output from the parametric studies yielded the following conclusions:

(i) Adding mass to the DMSA table decreases the tables' final velocities after the second impact. The simulation shows the peak impact acceleration of the second impact decreases by 15% as the DMSA table mass increases by 100%. Therefore, when conducting experiments with this accessory the fixture mass on the DMSA table should be minimized to the extent possible. The manufacturer could also decrease the thickness of the DMSA table to produce higher accelerations at lower drop heights. However, it's important to make the table thick enough to keep its natural frequencies well above the impact frequencies.

(ii) The rebound springs have negligible effect on the time response of the table. However, high drop counts have caused the spring to break. Increasing the stiffness of the springs could prevent failures in the spring, but the spring force will then oppose the movement of the DMSA table and reduce the peak accelerations.

(iii) The clearance between the DMSA table and the DMSA base directly correlates with the time to their impact. Thus, the peak accelerations of the secondary impact in the simulation increased slightly as the clearance

decreased. However, in the experiment this effect could be amplified due to drag caused by friction along the guide rods.

2.3 General conclusions

The DMSA accessory allows for very high impact accelerations through secondary impact. Using a model, created in FEA, different parameters were modified to examine their effects on the acceleration-time response. Through this process, much was learned about modeling contact, dynamic simulations, and optimization techniques for drop testing applications. This global model can provide boundary conditions for sub models in the absence of experimental data. As an example, this global model can provide boundary conditions for local PWB models, when we are interested in modeling the history of shear strain rate and distribution in solder joints caused by high accelerations.

The results showed that the model can accurately capture the dynamics of the drop tower and the DMSA. Parametric studies were used to calibrate surface interactions in the model to match the experimental data for a 15 in drop. It was determined that defining a soft contact interaction for impact between the DMSA table and the DMSA base adequately mimicked the role of the pulse-shaper sheets between them and produced an acceleration response similar to experimental data. A hard contact interaction was used to describe the impact between the drop table and the elastomer pulse shaper, since the compliance and damping of the elastomer cylinder is explicitly included in this model.

In analytical models and parametric studies of different structural definitions, design suggestions can be offered to the experimenter. First, as shown in previous works by Kelly et al [8], the simple analytical studies shown in Section 2.2.1.2, provide the

sensitivity of the impact acceleration magnitude to added mass on the DMSA table (e.g. due to fixture and specimen mass). Therefore, a specimen fixture should be as small and light as possible. Furthermore, analytic models show that decreasing the stiffness of the pulse shaper under the drop table, currently elastomer, can increase the amplification factor generated by the DMSA.

Overall, this test setup can be use to conduct drop tests at very high impact accelerations. Currently, preliminary testing for product bench marking and qualification at accelerations ranging from 10,000 G to 30,000 G has been completed and will be discussed in Chapter 3. Secondary impact has been further exploited in Chapter 3, to further amplify the impact accelerations through impact between a printed wire assembly (PWA) test specimen and the fixture during a DMSA drop test. The FEA model of this additional secondary impact and its role in subsequent fixture design can be found in Chapter 3.

3 Simulation of board level drop tests with intentional board “slap” at high impact accelerations

This chapter will investigate high acceleration testing of printed wiring assemblies. Further study is done to investigate board “slap.” This can occur when high impact accelerations are applied to the clamped portions of the board and the board is allowed to impact the test fixture. This documented in the literature but not specifically investigated.

3.1 Introduction and problem statement

Developers of handheld consumer products are increasingly introducing sophisticated and innovative functionalities utilizing state-of-the-art technologies. Devices with touch screens, MEMS gyroscopes, and accelerometers have flooded the consumer market due to high demand. With increased functionality has come an expectation that the size and weight of the product will continually reduce. Therefore, internal structures such as printed wiring boards (PWBs) are becoming more slender, thus increasing the likelihood of unintentionally causing contact between the PWB and other internal structures like battery compartments, displays, and other circuit cards, or the interior of the case [1], [2].

In a paper focused on full product impact testing, Goyal et al. [1] and Askari et al. [2], concluded that secondary impact on against the case of a portable device can be one of the causes for internal structures to experience highly amplified contact stresses and accelerations and cause damage to the subsystems Furthermore, lighter mass subsystems (e.g. PWBs) can experience higher velocity changes if contact is made with heavier and

stiffer objects (e.g. casing, battery pack, etc.). In this paper, the velocity and acceleration of different locations on a test PWB will be investigated to determine its response to the magnitude of the impact with the fixture during drop testing on a drop tower equipped with a dual mass shock amplifier (DMSA).

Implementing design to cushion the impact, to restrict motion, or to allow free movement by increasing clearance are the best options to prevent impact damage [24]. Impact forces and full-field responses are difficult to model and product design is typically done by modeling only local effects [1]. This paper aims to provide some understanding regarding the impact accelerations at different locations along the span of a test board through dynamic finite element models. In particular, the focus is on secondary impacts, which refers to subsequent impacts between multiple masses in a system after the system has been subjected to an event like a drop or impact.

Secondary impact has been explored in previous works to investigate optimization techniques for generating very high accelerations for bench mark testing and qualification of electronics in harsh environments [13]. Similar techniques can be applied when investigating secondary contacts between internal structures of electronic systems if they have insufficient room to freely vibrate. The time and frequency response of a suspended mass (in this paper a PWB) are directly related to the impact pulse at the suspension point and the natural frequencies of the suspended mass [25], [26], [27].

The layout of this chapter is as follows. The test specimen and test fixture will be described in detail with emphasis on design features and pitfalls, in section 3.2.1.2. A FEA model will be used to describe the dynamic response of the test specimen and

fixture, and the results will be explained in section 3.2.3. Suggestions will be provided to minimize the acceleration level generated by impact.

3.2 Approach and parametric studies

In this next section, fixtures for high acceleration testing are introduced. Test fixtures to intentionally generate impact between specimens and fixture are also described. FEA simulations are used to predict the acceleration response of a PWB impacting a hard surface.

3.2.1 Test setup

The test is conducted on a commercially manufactured drop tower described in Chapter 2. A full description of the capabilities of the drop tower system can be found in Section 2.1. Conventional drop test standards usually do not provide specimen and fixturing guidelines for very high impact accelerations. JEDEC standards [9] for board level drop tests address impact acceleration pulses of 1,500 G with 0.5 ms duration and 2,900 G with 0.3 ms duration. The amplified impact acceleration pulses generated by the DMSA start around 10,000 G with 0.1 ms duration and can reach magnitudes as high as 100,000 G. The increase in acceleration levels may cause premature failures of the test PWA, due to excessive stress at the mounting holes in the four corners recommended in the standard JEDEC test. Figure 23 shows a typical PWB specimen used in JEDEC drop tests. The 4 corner holes are for the screw mounts to the drop fixture, and these are the areas of stress concentration discussed above. Therefore, in this study, a custom test coupon and fixture were designed and simulated in FEA and tested experimentally. The simulation, tests results, and design iterations are described in the remainder of this chapter.

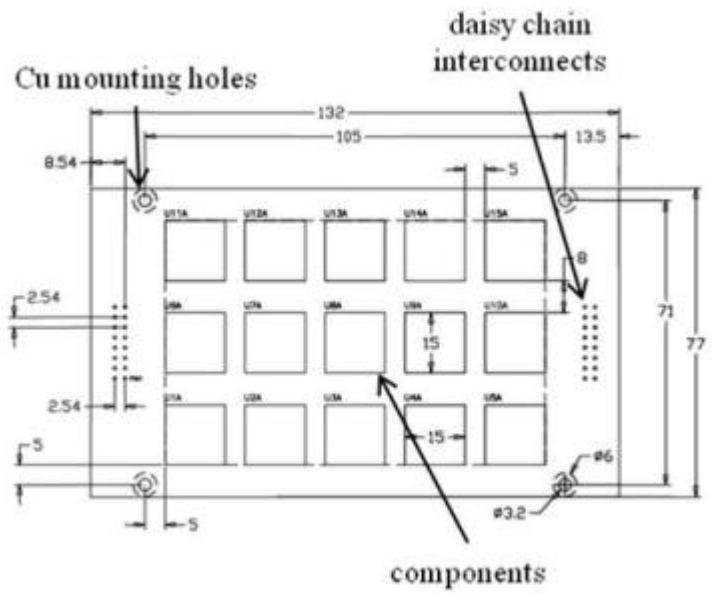

Figure 23: JEDEC standard for board level drop test [9].

3.2.1.1 Test specimen

The test specimen was designed to investigate the effect of impact loading on the durability of the components and interconnects on the PWB. Impact has the potential to create three sources of stresses on the component interconnects: (i) dynamic PWB flexure, (ii) inertial forces caused by the component mass and acceleration; and (iii) stress waves generated by secondary impacts between the PWB and the fixture. Secondary impact not only creates the third source of stress listed above, but also amplifies the first two.

The test vehicle uses built-up multilayer technology using a 2+4+2 stack-up (symmetric layup: 1 layer Cu plane with pads, 1 layer Cu plane with buried traces, 2 layers FR4). The test matrix included specimens with two different PWB thicknesses: 0.7 mm and 1 mm. The in-plane dimensions of the card are approximately 50 mm x 100 mm and the components are located along the x and y center lines, as seen in Figure 24. The specimen is clamped along the two short edges, using fixtures discussed later in

Section 3.2.1.2. The components placed on the x centerline, each experience different flexure and acceleration levels during a drop event due to the x-curvature (e.g. in the first mode). The components along the y-centerline all experience approximately the same load levels for mode shapes that have only x-curvature.

The test PWB is designed to accept six 49-I/O wafer level chip scale packages WLCSP49 and six MEMS components, totaling twelve components per board. The WLCSP49 components are daisy chained and electrically monitored for resistance jumps (in excess of 300 Ω) due to failed interconnects. The MEMS components are individually monitored every 25 drops to check functionality. To prevent trace failures, all traces have been buried and made thicker, and sharp angles have been avoided. The solder pads are non-solder mask defined, to further ruggedize the interconnects for drop durability [28].

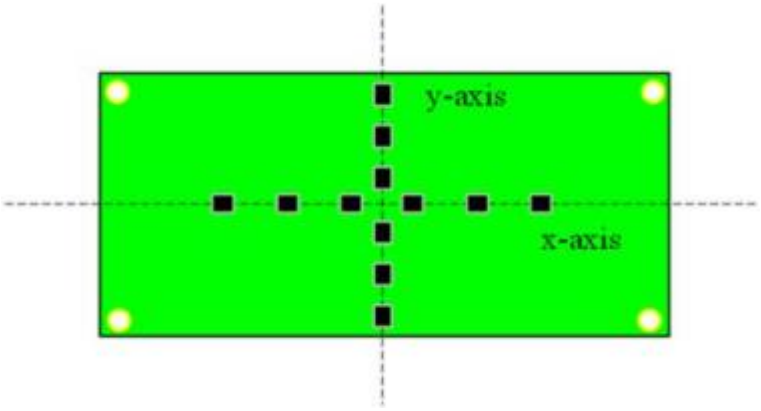

Figure 24: Test specimen with locations of components marked.

3.2.1.2 Test fixture

The fixture was designed to clamp the test PWB along the two short edges, with a 71 mm span between them. The dimensions and bolting foot-print were specifically selected for the test vehicle, drop and DMSA tables used in this study. Adapter plates to

alter the bolt pattern are avoided since their mass will cause an unacceptable increase in the total weight on the DMSA table and hence lower the acceleration ceiling generated by secondary impact [13]. Prior to detailed fixture design, preliminary FEA, as seen in Figure 25, was conducted on a simplified model of the test PWB. The material properties used in this model can be found in Table 4. The effect of unsupported spans below the PWA were explored to find unwanted high stress concentrations. Analysis showed extreme strain and board deformation at the board edges at very high accelerations. The test fixture went through two design generations to improve the fixture functionality and drop-to-drop repeatability. Details of the function, design, and pitfalls of the 1st generation fixture are provided in Appendix I.

Table 4: Orthotropic material properties of the PWB used in FEA

E_1(MPA)	E_2(MPA)	E_3(MPA)	G_{12}(MPA)	G_{21}(MPA)	G_{13}(MPA)	G_{23}(MPA)
19000	19000	9000	3700	3700	2900	2900

ν_{12}	ν_{21}	ν_{13}	ν_{23}	ν_{31}	ν_{32}
0.14	0.14	0.39	0.39	0.18	0.18

The 2nd generation fixture was re-designed to correct the problems caused by bending of the top clamp in Generation 1 (see Appendix I), and to improve testing quality. The top plate was made thicker and FR4 washers were used under the clamping bolts, to prevent the upper clamp from bending under the force of the bolts. The top and bottom plates were simultaneously secured to the DMSA table with the same bolts, to

reduce relative motion and setup time. Cavities were added to the edges of the clamp to route the wires used for monitoring daisy-chain net resistance.

Similar to the first generation clamps, multiple configurations were created by varying the clearance between the PWB and fixture, to vary the severity of the secondary impact between the PWB and the fixture. A zero clearance configuration (Figure 26a), was developed with a continuous bottom plate to prevent any downward board deflection. Trenches were added along the x and y centerlines of the bottom plate, as seen in Figure 26a, to test PWBs with components facing down. An infinite clearance version was developed by making a cavity in the bottom plate (Figure 26c) to create a long (71 mm) unsupported span, thus allowing the board to deflect freely in both directions.

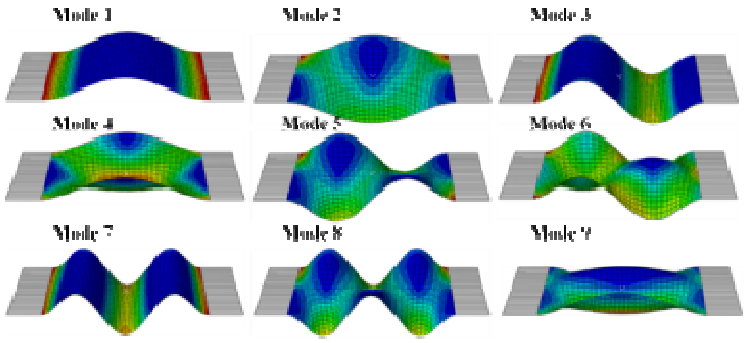

Figure 25: Board modes in the 2nd generation clamp.

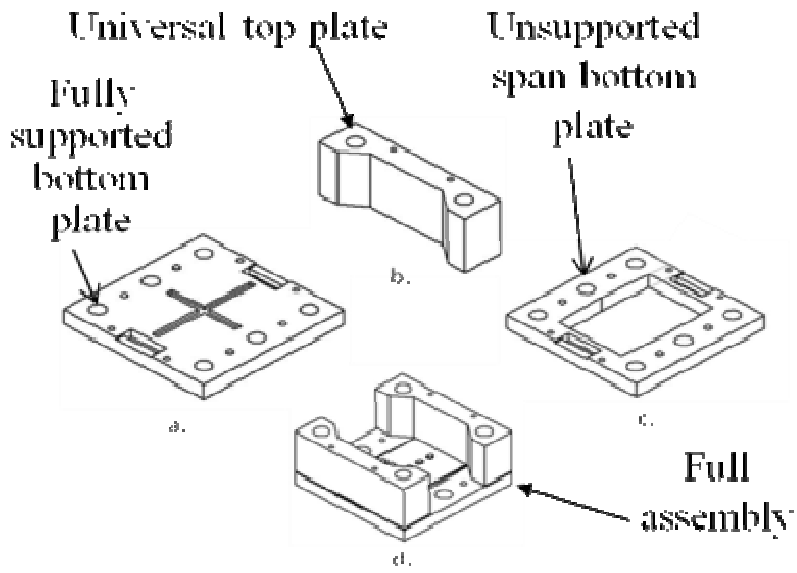

Figure 26: 2nd generation fixtures: a. zero clearance bottom plate clamp showing the trenches to accommodate components during face-down testing, b. universal top plate, c. infinite clearance bottom plate clamp.

In addition, finite clearance configurations were developed by the use of metal spacers (shown in Figure 27) of selected thickness between the PWB and the continuous back-plate. The purpose of the clearance is to allow the PWB room to gain velocity and impact the bottom fixture in mid-deflection, when the velocity reaches the maximum value. This secondary impact amplifies the PWB accelerations well beyond that of the freely deflecting configuration infinite clearance configuration. This amplification is based on the same secondary impact principle as that of the DMSA table. The spacer thickness was designed to maximize the velocity change (and accelerations), based on FEA results similar to that shown in Figure 28. Details of the FEA modeling are presented later in Section 3.2.3 of this paper.

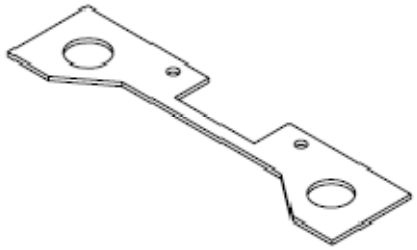

Figure 27: Spacer used to create a cavity under the board.

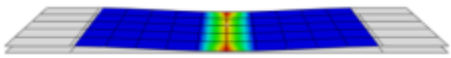

Figure 28: PWB impacting the fixture due to deflection in excess of the clearance created by the metal spacer to create a cavity.

3.2.2 Simple analytical model

In a paper by Wong et al. the response of board was derived for a simply supported beam [29], [21]. This paper will use a portion of this derivation to model contact between the PWB and the fixture and back out the impact force as an initial condition in an analytic two DOF model. This section will only use a portion of the derivation, the deflection, to model contact between the PWB and the fixture and back out the board response to be analyzed. A_o, Ω, ω_n, and w are the acceleration amplitude; frequency of the applied boundary conditions as seen in Section 2.2.1.1, resonant frequency of the PWA specimen, and deflection of the PWA, respectively. The deflection history at the center of the beam can be seen below in Equation 3.1. Damping was not included in this model since this paper focuses on the magnitude of the impact during the first half-cycle.

$$w(x = 0.5L, t) = \frac{A_o}{{\omega_n}^2}\frac{4}{n\pi}\frac{-\frac{\Omega}{\omega_n}}{1-\left(\frac{\Omega}{\omega_n}\right)^2}\left(\frac{\Omega}{\omega_n}sin\Omega t - sin\omega_n t\right)\sin\frac{n\pi x}{L} \qquad 3.1$$
$$n = 1,2,3 \ldots$$

The bending strain on the surface can be found if this equation is differentiated twice w.r.t. x and multiplied by half its thickness. The board center velocity and acceleration histories can also be found.

$$\dot{w}(x = 0.5L, t) = \frac{A_o}{{\omega_n}^2}\frac{4}{n\pi}\frac{-\frac{\Omega}{\omega_n}}{1-\left(\frac{\Omega}{\omega_n}\right)^2}\left(\frac{\Omega^2}{\omega_n}cos\Omega t - \omega_n cos\omega_n t\right)\sin\frac{n\pi}{2} \qquad 3.2$$

$$n = 1,2,3 \ldots$$

$$\ddot{w}(x = 0.5L, t) = \frac{A_o}{{\omega_n}^2}\frac{4}{n\pi}\frac{-\frac{\Omega}{\omega_n}}{1-\left(\frac{\Omega}{\omega_n}\right)^2}\left(-\frac{\Omega^3}{\omega_n}sin\Omega t + {\omega_n}^2 sin\omega_n t\right)\sin\frac{n\pi}{2} \qquad 3.3$$

$$n = 1,2,3 \ldots$$

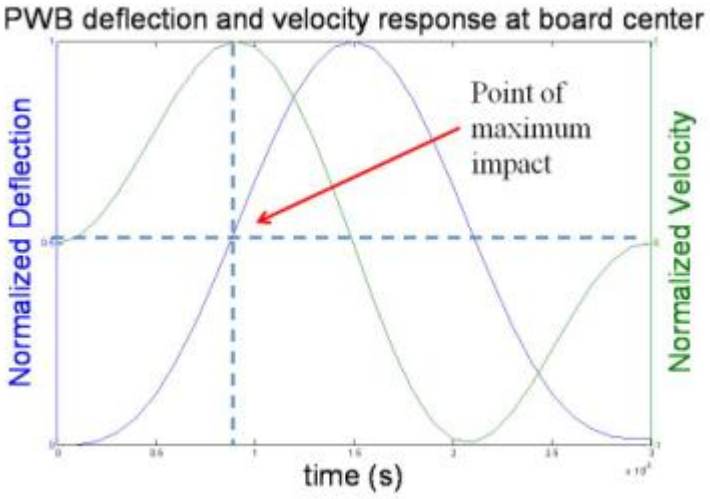

Figure 29: Normalized deflection and velocity histories at the board center.

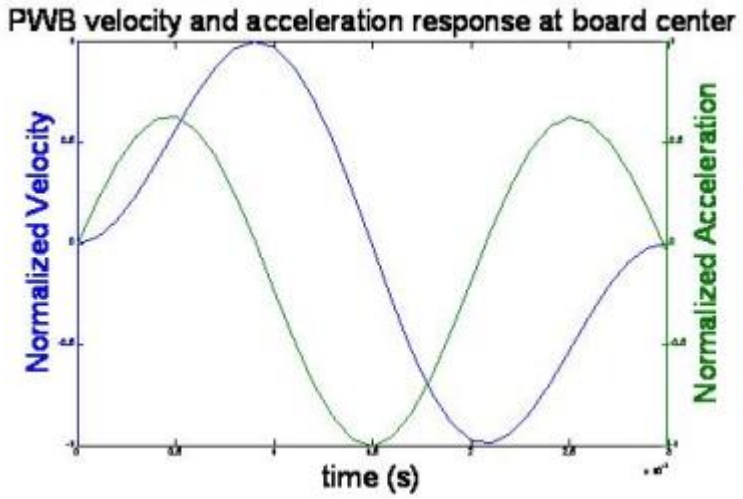

Figure 30: Normalized velocity and acceleration histories at the board center.

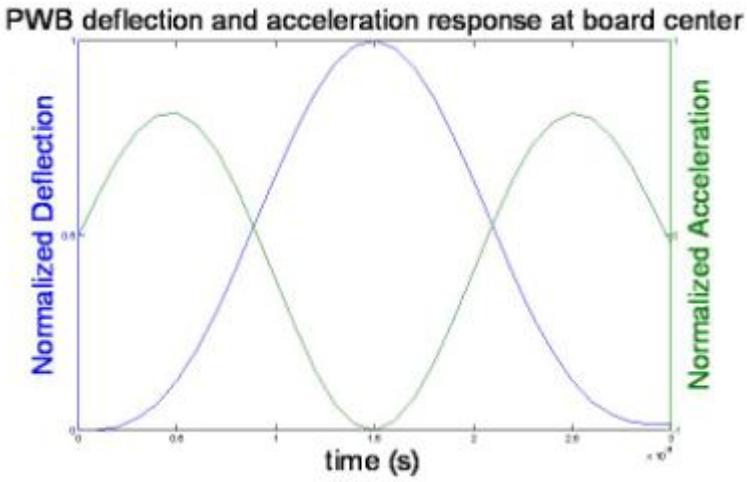

Figure 31: Normalized deflection and acceleration histories at the board center.

A closed-form solution for this problem is difficult, but the acceleration and deflection histories can be numerically analyzed as discussed later in Section 3.2.3. Figure 29, shows the first mode deflection and velocity time response at the center of a freely deflecting PWB with clamped edges. Comparing the board velocity to the displacement can provide insights into choosing a cavity depth that will produce the highest impact response due to maximum change in momentum of the board.

3.2.3 Input – G model overview

The literature is full of research conducted to understand the board strain transferred to the solder joints under drop loading [29], [28]. Impact between the board and the fixture causes high accelerations and early component failures similar those caused by secondary impact on the DMSA (discussed in Chapter 2). These boundary conditions have traditionally been avoided due to the added complexity caused by contact stress waves propagating through a fiber reinforced layup in the PWB. However, large amplifications caused by the board bottoming out can be exploited to shorten the test duration if all effects are carefully considered [13].

3.2.3.1 Model definition

The test board and fixture, as seen in Figure 32, were modeled [23] and analyzed using dynamic FEA. The test board material is defined with orthotropic shell elements of 0.7 mm. Thin PWBs have lower stiffness and this allows higher board deflections, thus increasing the amplification due to secondary impact. The portion of the board which is clamped is a partitioned section of the PWB defined with discrete rigid properties. The clamped ends of the test board are rigidly connected to the fixture, as seen in Figure 33. The continuous base, which the PWB impacts, is modeled as a rigid body. The contact interaction is defined as surface to surface kinematic hard contact because of the rigid body definitions in the model. The distance between the test board and the base fixture is modeled with the half thickness of the PWB, because the PWB was modeled with shell elements and have no physical thickness, plus some defined cavity depth. These definitions allowed the model to simulate the board impacting the test fixture under a drop load.

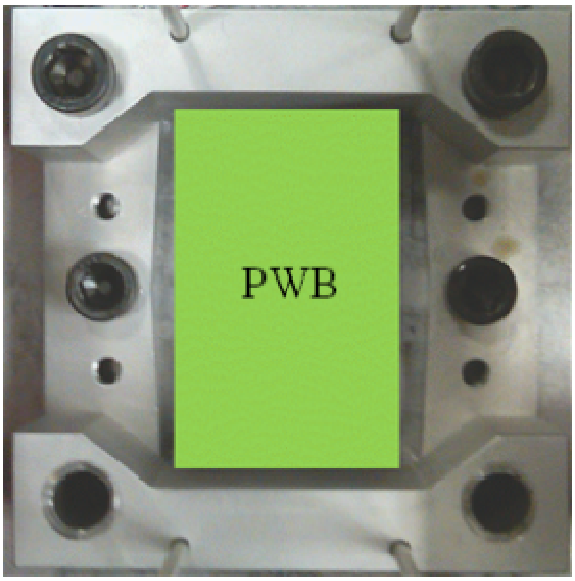

Figure 32: PWB mounted in Generation 2 fixture of Configuration 2.

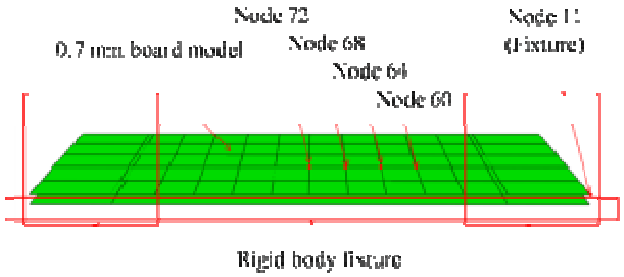

Figure 33: FEA model of deformable PWB and rigid fixture with a clearance in between

3.2.3.2 Cavity depth study

The clearance, between the test PWB and the fixture, was parametrically varied with FEA to understand the test board response as a function of the clearance depth. The impact accelerations generated by the secondary impact between the DMSA and the DMSA base and drop table are the inputs to the rigid boundaries of this local PWA model. Therefore, there is no relative motion between the rigid portions of the PWB and the rigid fixture base under the PWB. The acceleration response of the PWB is monitored along the center line of the test board at the labeled nodes shown in Figure 33.

3.2.3.2.1 Modal effects

The results of the sensitivity study can be seen in Figure 34. The vertical axis shows the maximum acceleration at the center of the PWB, normalized with respect to that of the freely deflecting (infinite clearance) configuration. The horizontal axis shows the clearance distance. The PWB impact amplification is expected to first increase due to increasing PWB velocity, as the clearance depth is increased from zero. Eventually, the amplification should pass through a maxima and decrease, as the clearance increases past the max velocity point of the PWB. The amplification should eventually disappear as the clearance exceeds the maximum deflection of the PWB at the contact location.

Instead, as shown in Figure 34, the amplification at the PWB center appears to disappear at about 0.6 mm, thus generating two local maxima at about 0.2 mm and again at 1.2 mm.

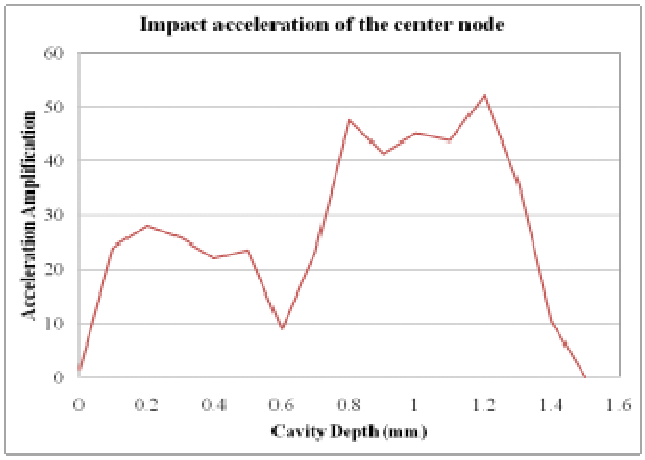

Figure 34: Acceleration amplification on the PWB w.r.t fixture acceleration, as a function of the clearance depth between the PWB and fixture bottom.

To understand the reasons for this "dead zone" at 0.6 mm, the test board was allowed to deflect freely. Figure 35 and Figure 36, show the displacement and velocity, respectively, at the nodes shown in Figure 24. The displacement plot shows that the center of the PWB is not always the lowest point as the board deflects after impact caused

by drop loading, because of multiple competing natural modes. Combination of the first and seventh modes causes reverse flexure at the center during some part of the deformation history, thus preventing impact at the center of the board.

Figure 36 shows the center node displacement, as well as the velocity of the center node and other freely deflecting nodes along the board's x-axis. At a deflection of approximately 0.6 mm, the center node loses velocity and is no longer the node with the highest velocity. This is because mode 7 displacement starts to oppose mode 1 displacement, and explains why the center of the board does not impact the fixture at this intermediate depth. Fixture designers need to be aware of such multi-modal contributions and possible "dead zones" when choosing a clearance depth for test boards. The displacement response at the clearance depths mentioned above can be seen in Figure 37.

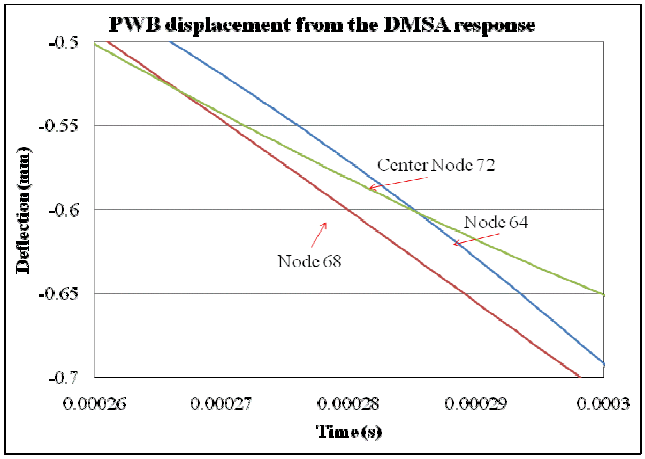

Figure 35: Close up of the displacements of sections of the PWB during from the DMSA response to a 15 inch drop.

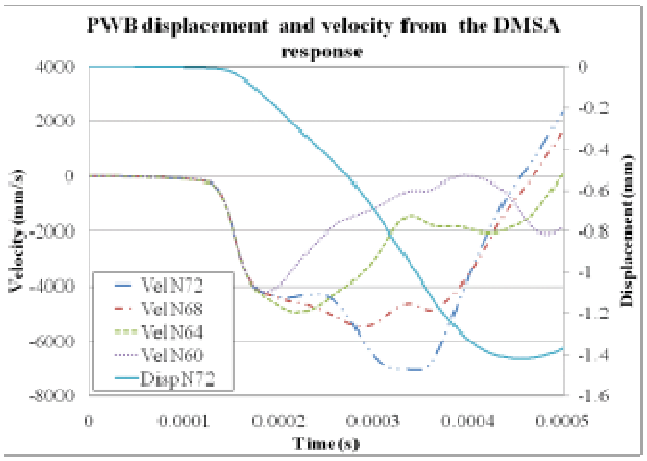

Figure 36: PWB displacement and velocity from the DMSA response to a 15 inch drop.

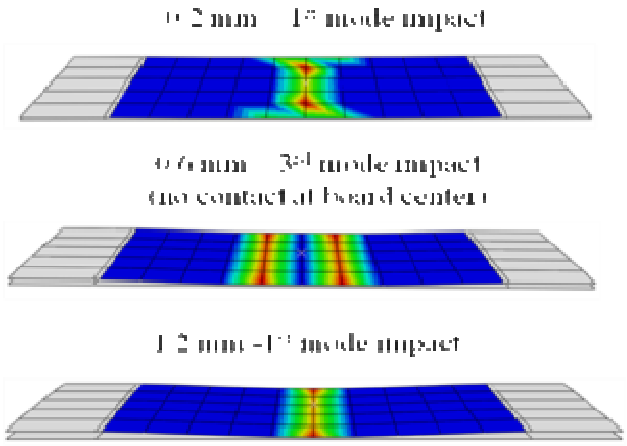

Figure 37: FEA contour of impact caused by different modes for a 15 inch drop.

3.2.4 Input – G conclusions

Purposefully causing contact between the test board and the fixture during a drop test can significantly amplify the impact at the point of impact even with a fully supported and tightly clamped PWB. Understanding the contact accelerations generated through impact can help ruggedize handheld products to withstand such events and also provide very severe test conditions for comparative analysis of different technologies. Contact between the test board and fixture during testing adds significant complexities for modeling and interpretation of the material interactions during the test.

From the results of the FEA sensitivity studies presented earlier, the relationship between clearance and impact amplification is a function of the PWB stiffness, and the drop height. The specific depth at which the magnitude of the impact will be greatest can be preliminarily determined by examining the displacement and velocity of a freely deflecting board. Competing modes dictate which parts of the PWB will make contact with the fixture base at each clearance height. The magnitude of the center node impact is caused by the momentum of the other board nodes. Figure 36 shows that at 0.2 mm cavity depth, the node velocities of the entire board are in phase, generating very high impact accelerations. However, immediately after, the node velocities start to diverge due contributions from higher modes and the impact severity decreases .

3.3 Conclusions

The standards put in place by JEDEC for drop testing may seriously underestimate the actual conditions in a drop event, especially when there are risks of secondary impacts between internal structures in the test specimen. Furthermore, the test fixture design recommended by JEDEC may induce unwanted failures at high accelerations due to material fatigue at the board corners. A special test fixture was developed in this study to reduce stress concentrations at these weak areas. The top plate of the fixture was designed to apply uniform pressure along the clamped edge of the test board. Clearances between the PWB and the fixture can be tailored to create very high or very low acceleration amplifications by exploiting secondary impact between the test specimen and the fixture. However, the relationship between the impact amplification and clearance is complex because of competing modal participation between multiple resonant modes of the test PWB.

While preventing board deflection and vibration in all directions may prove impossible, steps can be taken to reduce the magnitude of impact. Cushioning subsytems, with elastomer or other extremely compliant materials, to points at which contact is made can soften impact. Impact at a certain location can be prevented for a given drop height by tuning the clearance depth to a dead zone; however, in practical applications this is most likely unachievable due to manufacturing variability.

4 Specimen design and failure analysis from board level drop tests with intentional board slap at high impact accelerations

In this chapter, printed wiring assemblies (PWAs) are subjected to various drop accelerations and boundary conditions. The purpose of this section is to experimentally investigate high acceleration drop tests on component lifetime. The fixture types investigated will: prevent the PWA from deflecting downwards, allow the PWA to flex freely, and cause the PWA to impact the test fixture as described in Section 3.2.1.2. The impact accelerations tested are greater than prescribed by JEDEC standards [9]. The test specimen is a printed wiring board (PWB) that contains wafer level chip scale packages (WLCSPs) as seen Section 4.1.1.

4.1 Approach

The test fixture and specimen in this chapter were designed to imitate simulations in Chapter 3.

4.1.1 Test specimen

The test board for this test specimen has the same build up (2+4+2 Cu with FR4 core, with 0.7 mm or 1.0 mm thickness) as previously mentioned in Section 3.2.1.1. All of the boards discussed in this section are 0.7 mm thick. The test PWB is designed to accept Wafer-level-chip-scale-packages with 49 I/O (WLCSP49) and/or microphones based on Micro Electro Mechanical System (MEMS) technology. Six daisy chained WLCSP49 components are located along the length of the board, on the x-centerline, as seen in . These are numbered left to right as T7-T12. Due to the symmetry about the

centerline, T7 and T12 are near the edge of the unsupported span, T9 and T10 are nearest to the centerline, and T8 and T11 are at the intermediate locations. PWB flexure produced by mode one response (discussed in Section 3.2.1.1) is highest at the center components (T9/T10), followed by the edge components (T7/T12), and finally the intermediate components (T8/T11). On the other hand, the ranking of the accelerations (and hence of the inertial forces caused by the component mass) due to mode 1 response are different, with components at the center (T9/T10) experiencing the highest acceleration, followed by those in the intermediate locations (T8/T11) and finally those at the outer edges (T7/T12). To minimize spurious failures in the daisy-chain traces, sharp angles in the traces have been eliminated and thicker traces have been implemented in buried layers. Solder pads are non-solder mask defined.

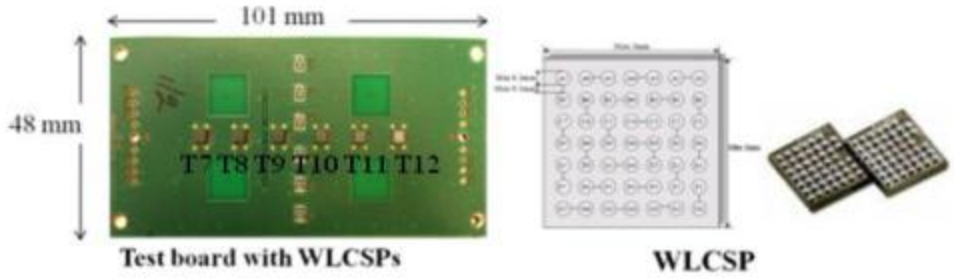

Figure 38: Test board with component locations and generic specimen design.

4.1.2 Test setup

PWAs with WLCSP49 (described in Section 1.1.1) components were tested at high impact accelerations, generated with the DMSA on the drop tower. The pulse magnitudes on the DMSA table ranged from 10,000 G to 30,000G with durations of 0.09 ms to 0.05 ms, as discussed in Section 2.1. The specimens were tested with the ruggedized 2nd generation fixture described in Section 3.2.1.2. The configurations tested are shown in Table 5 and include: zero clearance (fully supported PWB), infinite

clearance (fully unsupported 71 mm span), and finite clearances of various magnitudes (PWB separated from a continuous base plate with spacers of defined thickness).

Specimens were repeatedly dropped at required acceleration levels (shown in Table 5), until the daisy-chain failed. Failure was defined by loss of electrical continuity in the daisy-chain and was monitored with an event detector with a resistance threshold of 300 Ω. Drops to failure were recorded for the entire test matrix. As shown in the test matrix (Table 5), some boards were dropped with the components facing downwards and some with the components facing upwards. This changes the combination of the stresses generated by PWB curvature and those generated by the inertial forces arising from the mass of the component. For example, in the center components (T9/T10), the highest loading amplitude during a drop test (first half cycle), is a convex PWB flexure combined with a tensile inertial force in the face-down orientation, but concave PWB flexure combined with a compressive inertial force for the face-up orientation. The reverse is true for the edge components (T7/T12) for mode 1 response.

Table 5: Tests conditions for WLCSP49 drop testing.

Board #	G (x1000)	clearance (mm)	Component orientation
1-1	30	∞	Down
1-2	10	∞	Down
1-3	20	∞	Down
2-1	25	∞	Down
2-2	20	∞	Down
2-3	20	∞	Down
3-1	20	∞	Down
3-2	20	∞	Up
3-3	20	∞	Up
4-1	20	∞	Up
4-2	20	∞	Up
4-3	20	∞	Up
5-1	20	∞	Up
5-2	20	∞	Up
5-3	20	∞	Up
6-1	20	1.2	Up
6-2	20	1.2	Up
6-3	20	0.2	Down
7-1	20	0.2	Up
7-2	10	0.2	Down
7-3	10	1.2	Down
8-1	10	1.2	Up
8-2	10	0	Down
8-3	20	0	Down

4.1.3 Test results

Weibull analysis of the failure data was conducted to determine the repeatability of the tests and to compare the effects of different test parameters (component orientation, fixture type, and acceleration levels). All Weibull plots are catalogued in Appendix I. In Figure 39 and Figure 40, the time to failure of different board orientations, with components facing up vs. down, are compared. Data from symmetric component

locations are combined in the same Weibull plot (corresponding Weibull plots can be seen in Appendix B). Figure 39 shows that the failure mechanisms for both upward facing and downward facing components are likely to be similar for the edge components near the clamped edges of the PWB (components T7/T12), as indicated by the similar shape parameter values. However, the characteristic life for downward facing components is approximately 50% higher for the components at the edge of the board than at the center of the board as seen in Figure 40. Moving inward towards the PWB center, the components at intermediate locations (T8 and T11) show significantly different slopes indicating that failure mechanisms for face up vs face down orientations may differ, as seen in Figure 39. In contrast to the edge components, the characteristic life for face down assemblies is 13% lower in these locations. The two center components (T9/T10), as seen in Figure 39, have similar shape parameter values indicating similar failure mechanisms for different component orientations. The characteristic life for the face down configuration is 20% lower in these components.

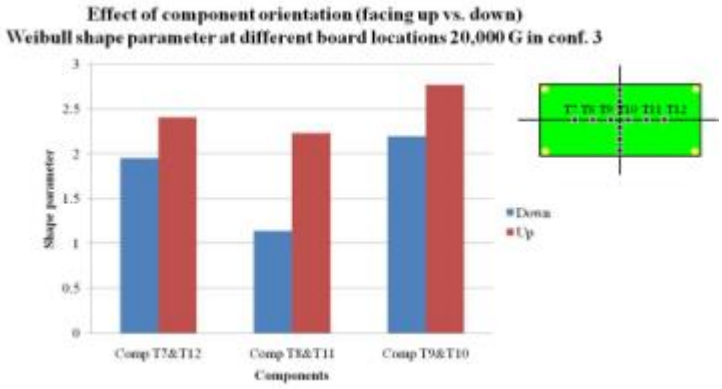

Figure 39: The effect of board orientation on variability of failure data at different PWB locations for a 20,000 G drop with finite clearance fixture.

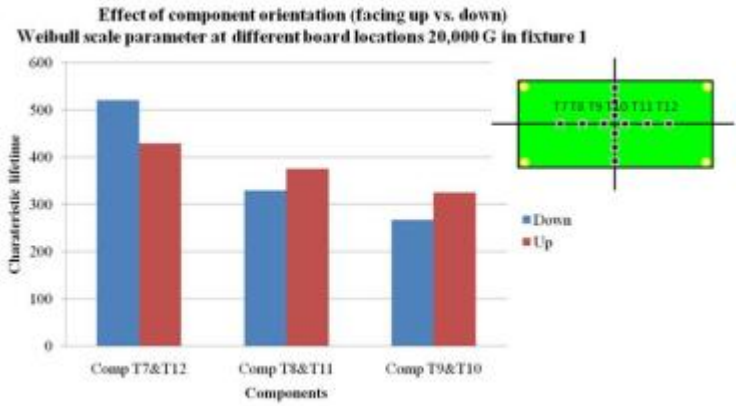

Figure 40: The effect of board orientation on component lifetime for 20,000 G drop in infinite-clearance fixture.

Unfortunately, due to high drop counts, a broad test matrix, and limited test materials, the tests could not be replicated sufficiently enough to produce statistically significant conclusions. However, there are some strong qualitative indications. Figure 40 reveals that at 20,000 G, in a freely deflecting PWB, center components fail first, followed by the intermediate components and finally by the edge components. This sequence correlates well with the inertial force magnitudes but not with the PWB curvature magnitudes. This suggests that the stresses due to inertial forces may be more influential in these studies than those due to PWB flexure. Figure 41 compares the inertial force and the board curvature with the component lifetime. Components fail faster at higher impact accelerations for the boundary conditions used in these tests. For example, Figure 42 shows that the durability of down-ward facing components near the center of the board does correlate with the drop acceleration magnitude, with tests showing earlier failures at 25,000 G and 30,000 G than at 20,000 G. However, at accelerations greater than 20,000 G, permanent inelastic bending was observed in the PWB. Possibly due to this reason, the characteristic lives for the 25,000 G and 30,000 G tests do not show clear trends, as seen in the intermediate components in Figure 42. Figure 43 confirms that secondary impacts between PWB and fixture can accelerate the

damage accumulation rates. In downward facing boards tested at 20,000 G with 0.2 mm and 1.2 mm clearance, failures in the center components occurred significantly earlier in cases with secondary impact between PWB and fixture, compared to cases with free deflections. This trend correlates well with the impact response predicted for these cases by FEA transient analysis in Section 3.2.3. Similar trends are observed for face up configuration.

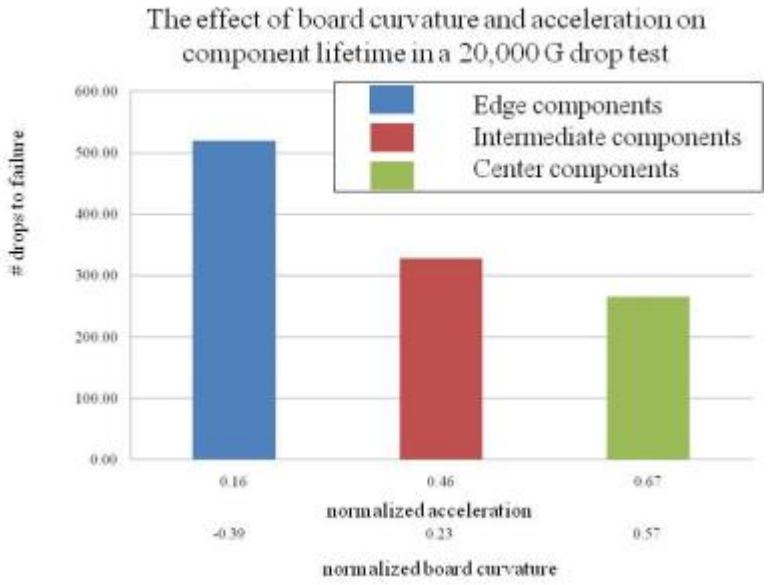

Figure 41: The component lifetime compared to the acceleration and curvature at the component site.

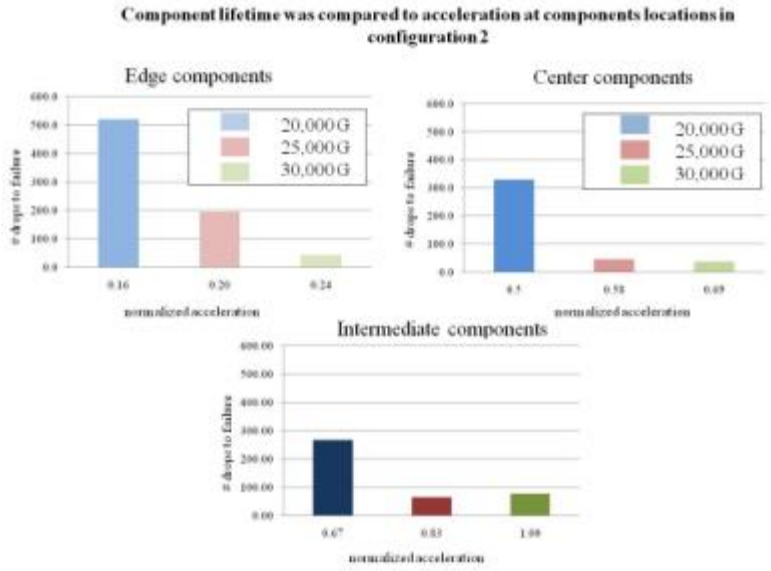

Figure 42: Component lifetime at different board locations with varying magnitudes of impact.

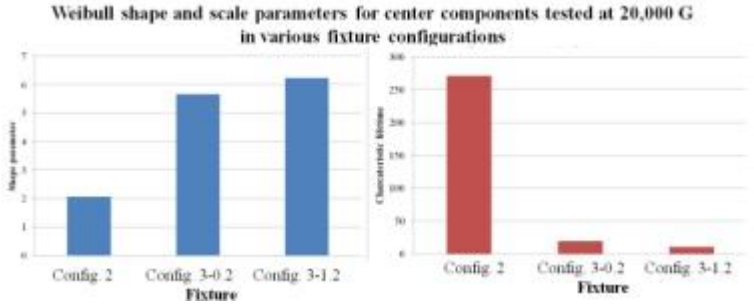

Figure 43: The effect of fixture configuration on component lifetime and failure mechanism.

4.1.3.1 Failure analysis

Components, identified as failed, due to resistance increase measured by the event detector, were mounted in epoxy-resin and cross-sectioned. Traditional dye and pry techniques were also used, but did not provide enough resolution to determine failure sites. Figure 44, Figure 45, and Figure 46 show the results for different test conditions. Typically cracks in cross-sectioned specimens are wide enough to observe using an optical microscope. However, in some cases, a scanning electron microscope (SEM) is used when further magnification is required. In some cases lateral cross-sectioning was

used to look for trace cracks; however, multiple specimens indicate that traces do not fail in these test boards.

4.1.3.2 Failures in infinite-clearance configuration:

The failure sites varied depending on the testing conditions. At 20,000 G, test boards that are allowed to deflect freely (infinite clearance), and experience fatal cracking mostly seen in the interfacial layer of intermetallic compound (IMC) towards the component. Failure analysis (FA) of this test condition can be seen in Figure 44. Board 4-1 was subjected to 100 drops and failure occurred in component T9 approximately at 68 drops. The fatal crack occurred in the IMC layer near the component interface, as seen in the SEM image. The location of the failure site for this component can be seen using the bump locator in Figure 44. Board 1-3 was subjected to 360 drops and the component T10 failed after 80 drops. Unfortunately, additional post-failure drops after failure can destroy evidence about precise failure modes. Similar to the previously mentioned board, fatal cracks were observed at the IMC layer near the component interface. Cracking was also observed in the IMC layer near the PWB Cu pad. Tests at 10,000G did not produce failures in the freely deflecting configuration.

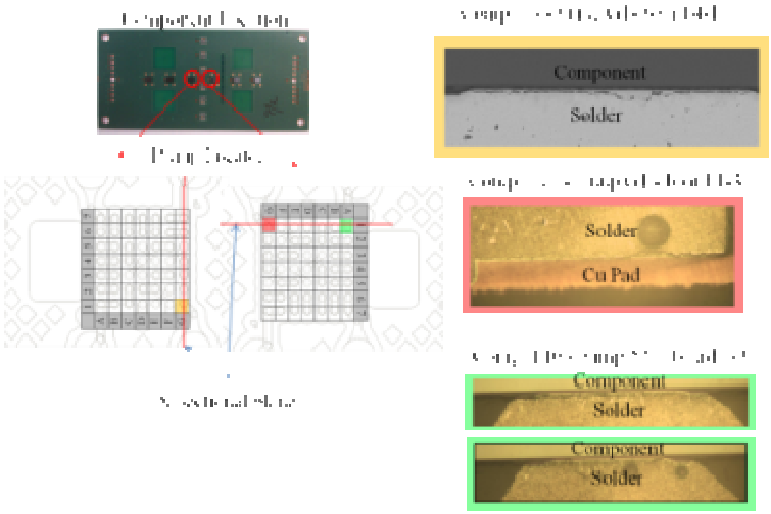

Figure 44: FA for boards 4-1 and 1-3 at 20,000 G in zero-clearance configuration (ref. Table 5 for component orientation).

4.1.3.3 Failures in finite clearance configurations

Boards allowed to impact the fixture but with various clearance depths, experienced cracking predominately in the interfacial IMC layer near the PWB pad. Figure 45 and Figure 46 shows the FA for configuration with 0.2 mm clearance, 20,000 G. In Figure 45 , component T10 on Board 6-3 failed at 16 drops and was subjected to 24 drops with 0.2 mm clearance. Cracks, fatal and partial, can be seen in the interfacial IMC layer at both the PWB and component pads of the solder joint. However, as seen Figure 46, FA of the same component and board at different cross-sectional planes, show that fatal cracks mostly occur at the Cu pad on the PWB. Pad peel-out was another failure mechanism observed multiple times in impact testing, but was not as predominant as IMC cracks at the component corners. When the acceleration was reduced to 10,000 G and tested with a clearance of 0.2 mm, 5 out of 6 components facing downwards failed. When the clearance was increased to 1.2 mm, 10,000 G tests failed only the two inner components near the PWB center (T10/11). The same drop condition failed to produce

failures within 500 drops, when the components faced upwards. Therefore, component orientation can clearly have a strong influence on drop durability.

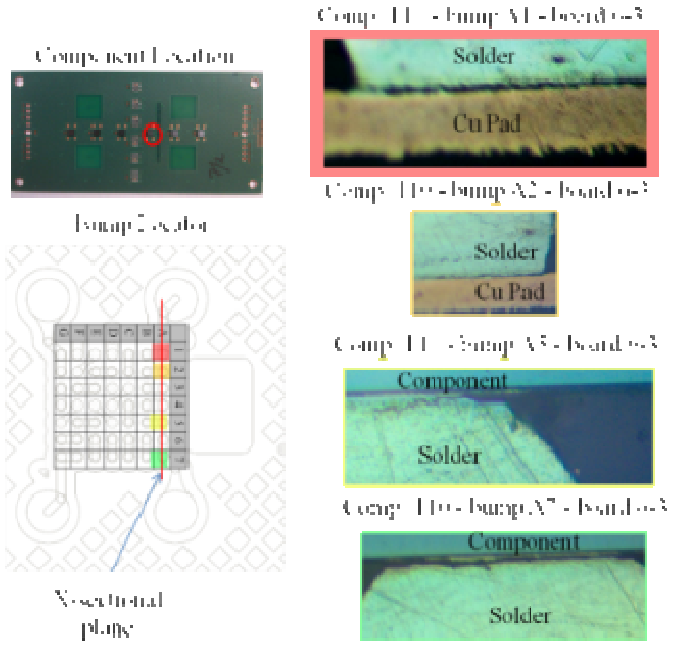

Figure 45: FA for board 6-3 at 20,000 G in finite clearance configuration (ref. Table 5 for component orientation).

4.1.3.4 Failures in zero-clearance configuration:

When the component was fully supported, failures varied with acceleration levels. Tests at 10,000 G with the components facing down did not produce any failures within 500 drops; however, at 20,000 G, 4 out of 6 components failed within 500 drops.

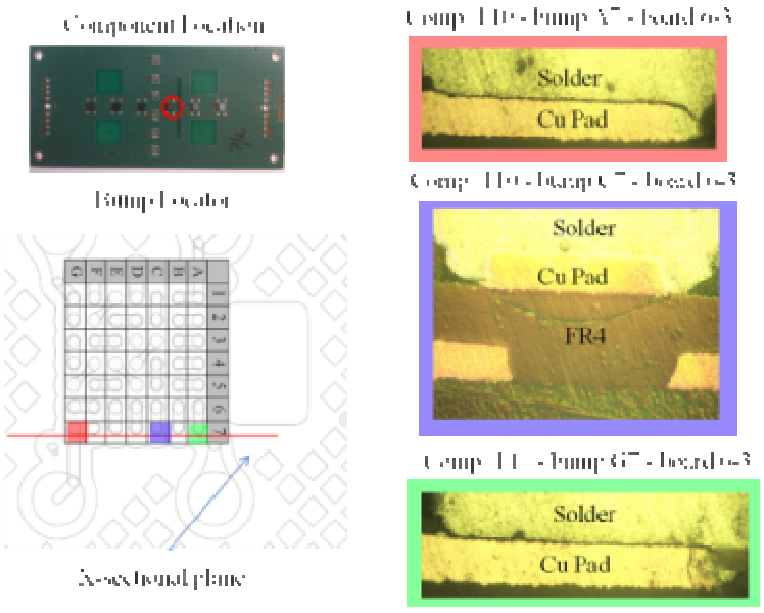

Figure 46: More FA for board 6-3 at 20,000 G in the finite clearance configurations (ref. Table 5 for component orientation).

4.2 Conclusions

Drop durability results provide clear indicators of the influence that board orientation, fixture style and impact accelerations have on the component lifetime. Due to the limited amount of data, the conclusions must be interpreted in a semi-qualitative sense rather than in a quantitative sense. In the tests where the board is allowed to freely deflect (infinite clearance configuration), fatal cracks are mostly seen in the interfacial IMC layer near the component. Impact accelerations in excess of 10,000 Gs had to be generated by the DMSA, to cause failures (resistance change in excess of 300 Ω) within 500 drops. Testing with a fully supported card (zero clearance configuration), where the board is prevented from deflecting downwards, impact accelerations in excess of 20,000 G were needed to cause all components to fail within 500 drops. When a clearance of x mm was provided between the board and the fixture to tailor the impact magnitude (finite clearance configurations), the failure rates increased. When tested at 10,000 G, with the

finite clearance configurations, a 0.2 mm clearance caused the majority of the components to fail. When the clearance was increased to 1.2 mm only the two inner components failed within 500 drops and in the component up orientation no failures were observed within 500 drops. The failure modes in the finite clearance configuration were predominantly fatal cracks in the interfacial IMC layer near the PWB. In a few of these tests, partial or full pad peel out was another observed failure mechanism. The clearance which produces optimal impact is clearly proportional to the drop height (impact amplitude) as explained in Section 3.2.3.2.

Weibull analysis provided insight to component time to failure as it is influenced by impact acceleration, board orientation, and fixture type. In freely deflecting (infinite clearance) configuration at 20,000 G impact accelerations, the component orientation had a ± 20% influence on the characteristic life of the components. Board orientation also had an effect on the slope of the Weibull shape parameter, indicating an influence on the failure mechanisms.

Statistical analysis showed a strong influence of secondary impact (between the PWB and the test fixture) between. While the data is statistically sparse, there is a strong qualitative indication that boards with finite clearance from the fixture, which were allowed to deflect downwards and contact the fixture, failed earlier than freely deflecting boards tested at the same acceleration level. This trend agrees with FEA conducted with similar boundary conditions, showing that the impact accelerations in the board at contact are as much as 50x higher than the input impact accelerations to the fixture.

The influence from increasing impact accelerations on component lifetime was also investigated. Again, the statistical data is sparse. However, as expected, there is a strong

qualitative correlation between fragility and impact acceleration level for boards which are allowed to freely deflect (infinite clearance configuration).

5 Summary and general conclusions

In the chapters presented in this work, the influence on secondary impact on drop acceleration and durability was investigated via simulation and experiment. Secondary impact is defined, in this thesis, as a subsequent impact initiated by a primary impact. A drop tower, with a moving drop table dropping onto a relatively hard surface, was used to produce the primary impact, generating impact accelerations as high as 5,000 G. The Dual Mass Impact Amplifier (DMSA), an attachment mounted to the drop table, produced secondary impact with impact accelerations reaching magnitudes of 100,000 G, using collisions between masses with opposing velocities,. The drop tower with the DMSA system was simulated using transient FEA, and parametrically investigated for sensitivity to design parameters.

Conclusions derived from studying secondary impact in the drop tower assembly were applied in drop testing electronic components. FEA provided insights for fixture and specimen design. Simulations of board level drops were modified to investigate further secondary impacts between the PWB and the fixture.

The conclusions from FEA spurred experimentation. Circuit boards containing MEMS microphones and WLCSPs were drop tested at very high impact accelerations using a combination of secondary DMSA impacts and further secondary impacts between the test PWB and the fixture. Drop durability was investigated for different impact acceleration levels and fixture types. Failure analysis was conducted and compared to existing industry research.

The conclusions of this work can be divided by chapter. In the second chapter regarding the drop tower and the DMSA, it was determined that FEA software can capture interactions between dynamic systems quite accurately. Furthermore, the parametric studies showed that adding mass to the DMSA table can reduce the peak impact acceleration.

In the third chapter, regarding fixture design for high impact accelerations and board slap, it was determined the amount the board is allowed to deflect, before it impacts the fixture, is directly related to the magnitude of the impact acceleration produced at the point of impact. FEA provided insight into the modal contributions on the magnitude of the impact, and predicted impact amplifications up to 40x the impact accelerations at the clamped portions of the board.

The fourth chapter concluded, through reliability testing, that impact between the board and fixture caused failures earlier than in a board allowed to freely respond. Reliability testing of the WLCSP showed that fatal cracks were most common in the corner ball of a component in the IMC on the component side. In MEMS testing, failure was seen in the wire bonds connected to the MEMS structure. This could be due to delaminating of the die adhesive holding the MEMS to the component substrate.

These conclusions all have secondary impact in common. High impact accelerations from the DMSA were the input to the input-G PWB model in the second chapter. Moreover, the DMSA and the impact fixture were used to conduct extremely high drop reliability tests in the third chapter. Thus, this paper is intended to provide useful knowledge regarding drop testing at very high impact accelerations.

6 Thesis contributions

This work contributes to the evolution of drop testing methodologies. Velocity amplifiers, the Hopkinson bar, and the DMSA are all capable of generating high impact accelerations via secondary impacts, and yet in-depth experimentation and simulation of these systems have not yet been published. Since there are commercial version of the DMSA system already available, it was not in our best interest to research design guidelines. Instead, research was conducted on an existing system to parametrically study the effect of different design parameters. The contributions of each chapter will be provided in an itemized list.

1. Simulation of secondary contact to generate very high accelerations
    - First FEA study of a commercial drop tower and DMSA, to demonstrate accurate representation of the dynamics of impact, and parametric study of test design (pulse shaping material, fixture design, and drop height).
    - Simulations of a drop test were demonstrated to provide accurate boundary conditions for more detailed local sub-models, without experimental data.
    - Insights into effective ways to model contact interactions in transient FEA for colliding masses.
2. Simulation of board level drop tests with intentional board “slap” for high impact accelerations
    - First FEA study of a test board with different boundary conditions to mitigate unwanted board dynamics (free edge deformation at connection sites)
    - Guidelines for the development of test specimens and fixtures for drop tests at extremely high impact accelerations well beyond prescribed industry standards.

- Fixture design for reliability testing to intentionally impact between test PWB and the fixture, in PWB-level drop testing.
- Insight into high impact accelerations produced when the board impacts the test fixture, at various impact velocities.
- Possible impact mitigation techniques (response dissipation through mode canceling, pulse shaping material), to prevent high impact accelerations.

3. Specimen design and failure analysis from board level drop tests with intentional board “slap” at high impact accelerations
    - Guidelines for failure monitoring of WLCSPs for short duration, high impact amplitudes.
    - Guidelines for test specimen design of circuit boards containing WLCSP49s for high impact accelerations.
    - Guidelines for failure monitoring of COTS MEMS microphones for short duration, high impact amplitudes.
    - Guidelines for test specimen design of circuit boards containing COTS MEMS microphones for high impact accelerations.
    - Statistical comparisons of MEMS and WLCSP49s component lifetimes in board level drop tests at different accelerations, fixture types, and component orientation.
    - List of common failure mechanisms in WLCSP49s and COTS MEMS for board level drop tests at high impact accelerations.
    - Comparisons between component lifetimes in freely deflecting circuit boards and circuit boards that impact their test fixture.

7 Limitations and future work

There were several limitations in the work described in this paper. First, the accelerations of the test board could not be accurately measured due to the mass of the high acceleration accelerometers available to consumers. Second, the frequency range of accelerometers is between 0-10 kHz, which truncates acceleration data at very high accelerations. Since the FEA models were calibrated to experimental data, this could affect the calibration of the contact parameters in the model. Third, the speed of the data acquisition system did not allow for inspection of the resistance trace as the board deforms in a 50 microsecond event. Fourth, external forces (such as aerodynamic drag and bearing friction) were not included in the drop tower model, limiting the simulation accuracy. Finally, the test boards in the FEA models of board impact were comprised of shell elements and did not account for PWB compression in the thickness direction and interaction between board layers.

Further research can address almost all of the limitations listed above. Significant board strain analysis has not been conducted. The test fixture and specimen can also be characterized in a sine sweep to determine the natural frequencies of the system. Accelerometer technology is constantly advancing; thus, the accuracy of the drop tower characterization can be improved. Furthermore, optical non-intrusive methods of monitoring board acceleration, and deflection will be investigated. Mounting instruments to a test specimen may affect its response in drop conditions. FEA models can be more detailed to include deformations in the PWB thickness direction and external forces to accurately match the experimental test conditions. Further research into reliability testing at high accelerations can be conducted to improve the statistical significance of the data

and conclusions. Failure analysis of the MEMS structures can be improved by creating an automated desoldering machine to reduce human error in the delidding process.

Appendix I Fixture development

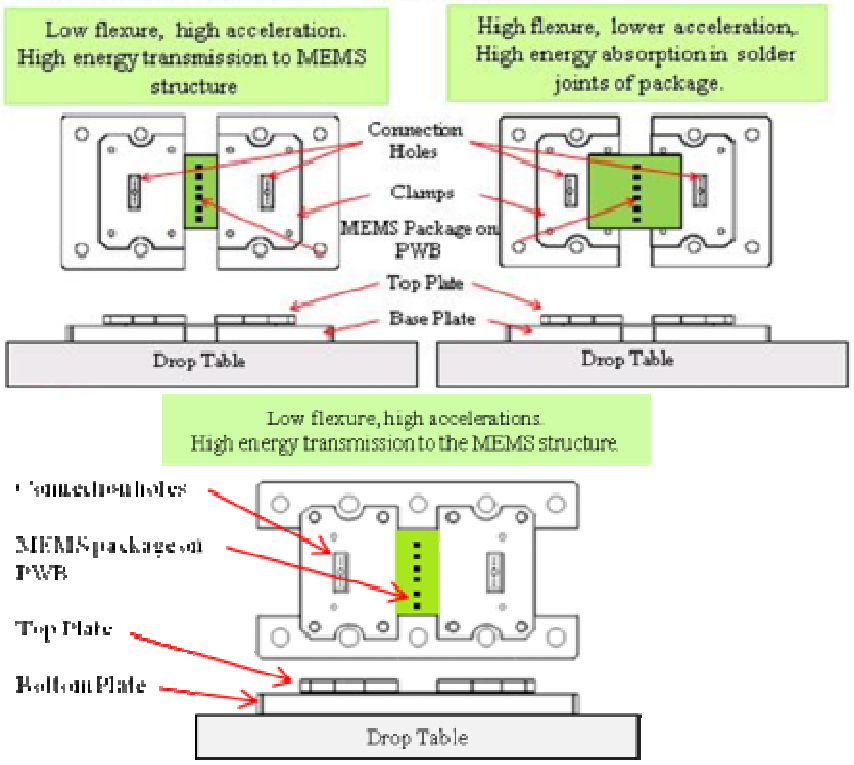

Figure 47: Fixture design: short span (left), long span (right), zero span (bottom).

The first generation fixture design did not behave as expected in testing. The top clamp was not sufficiently stiff and flexed under the clamping forces (as schematically shown in Figure 50), thus causing an asymmetric strain response due to board buckling along the width direction. Measurements recorded during the clamping process showed that the board strains are non-trivial in both directions (ε_x and ε_y), and their magnitudes are directly proportional to bolt torque. The bending strains on the PWB along orthogonal directions had opposite signs, thus producing a "saddle shape" from the clamping conditions. An exaggeration of this can be seen in Figure 48. Furthermore, each drop causes residual curvature possibly because of friction forces between the PWB and the

fixture. Figure 49 shows a cumulative buildup of curvature in each drop and then a release in the last drop as the cumulative flexural energy becomes substantially large.

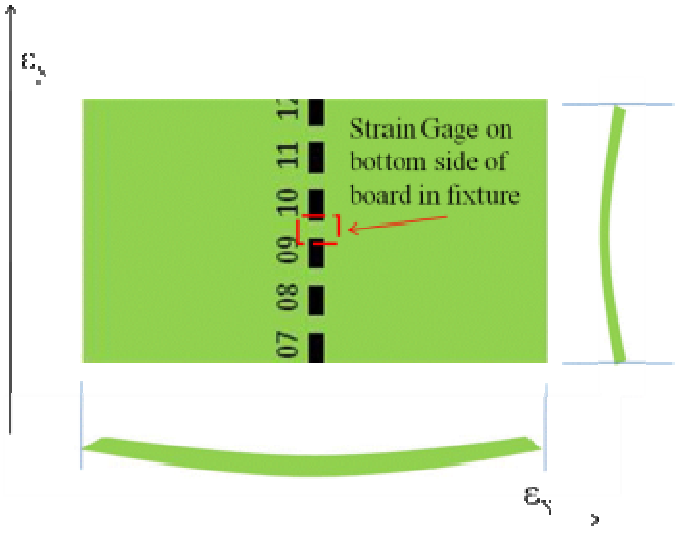

Figure 48: PWB assumes a "saddle" shape under the clamping forces.

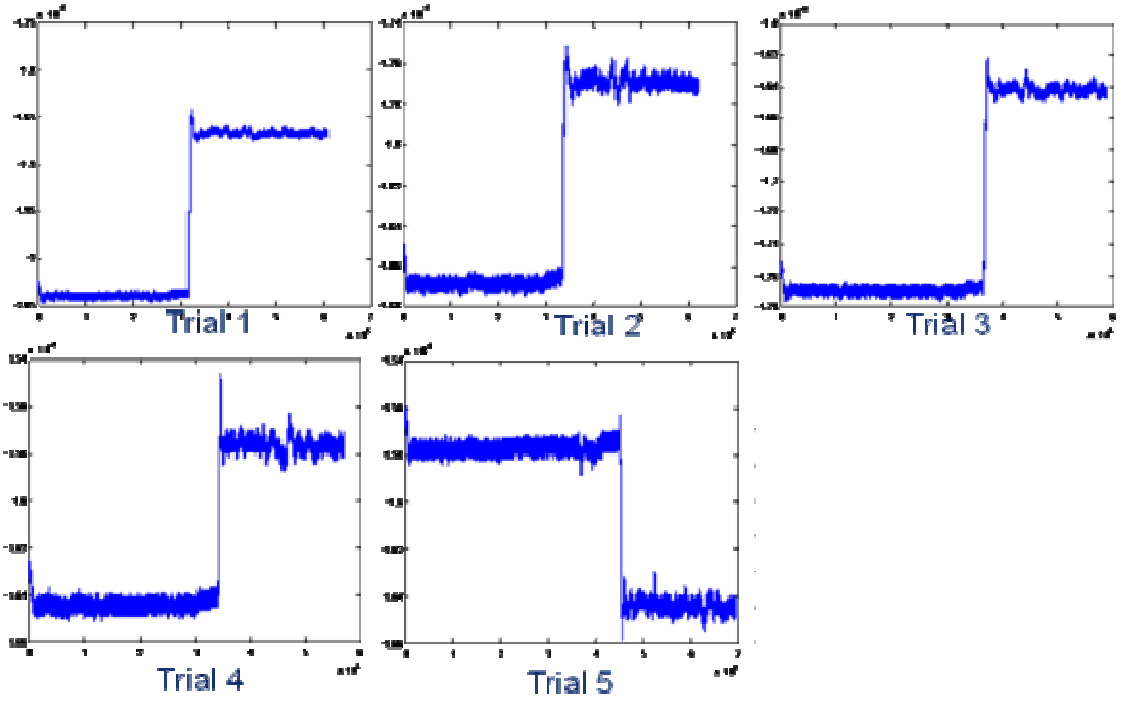

Figure 49: Residual strain accumulation with successive drops.

Three steps were taken to mitigate the pre-strain caused by the clamping process. First, steel alignment pins, to set the board in the correct orientation in the fixture, were used during bolt tightening and then removed before the test. Second, FR4 spacers were used under the fixture, outside the bolts, as seen in Figure 51, to prevent the top clamp from bending over the board during bolt tightening and create a uniform pressure on the clamped portion of the PWB. Figure 52 shows the reduction of asymmetry in the longitudinal strain of the test board during a drop test without FR4 spacers. Third, to counteract bending in the top clamp, two bolts were added to the fixture as seen in Figure 53. A comparison of the static board strain, seen in Figure 54, caused during fixture bolt tightening shows a difference of 500 με.

Figure 50: Effect of tightening the top clamp.

Figure 51: Use of PWB spacers can reduce beam bending in the top clamp.

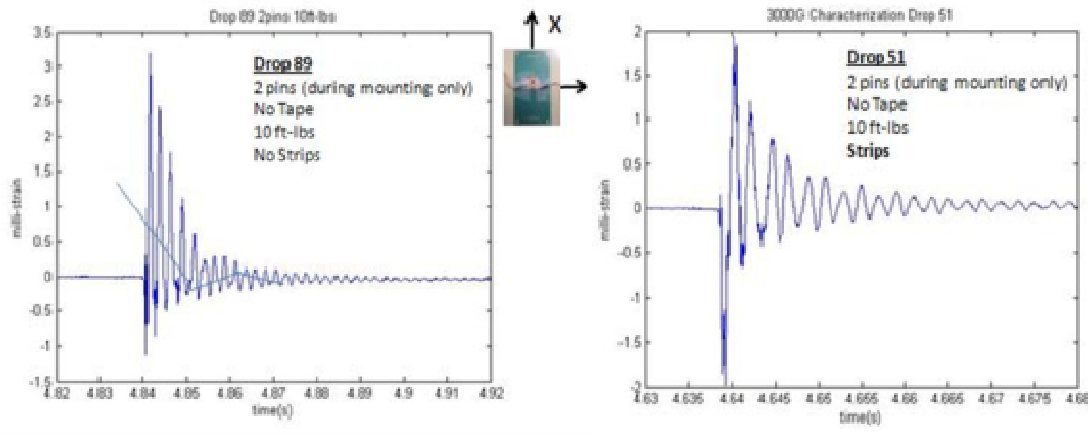

Figure 52: Strain history from a low acceleration drop (3000G) with and without spacers under the top fixture.

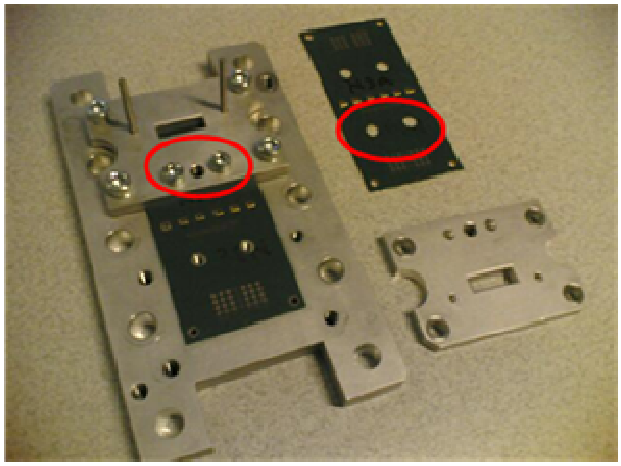

Figure 53: Fixture modification, showing center bolt, to minimize flexure of top plate.

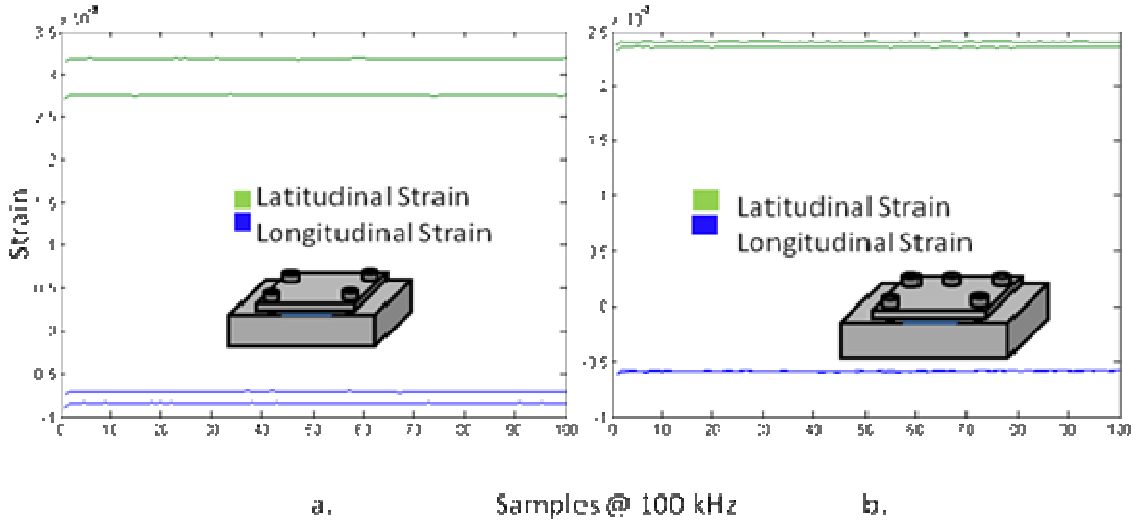

Figure 54: Static strain values from two tests of the top plate: a. without a center bolt, b. with a center bolt.

Appendix II Weibull analysis

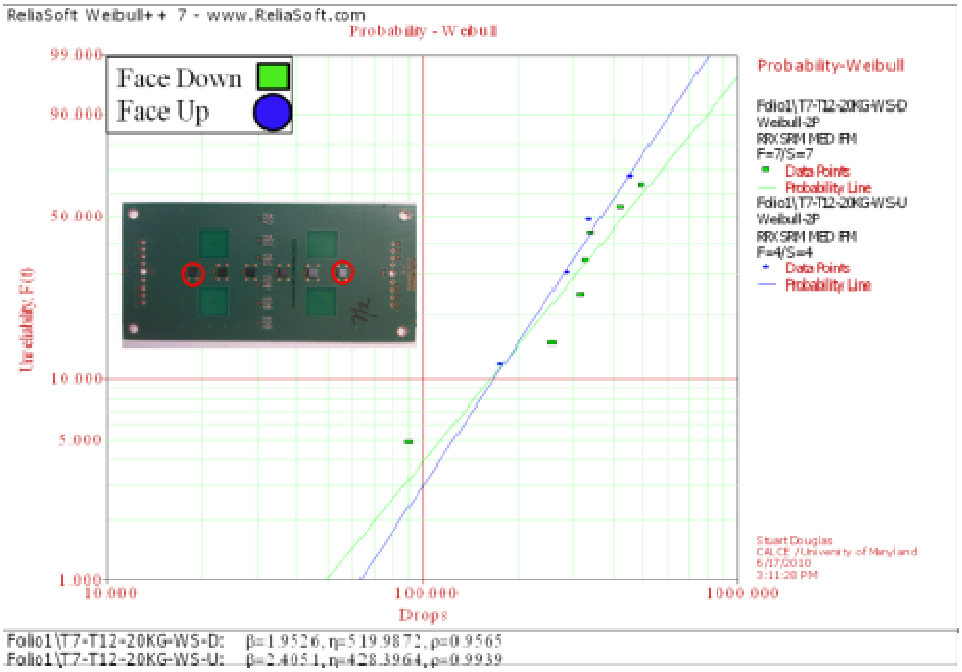

Figure 55: Comparison of outer component (T7 and T12) failure times with varying component orientation (in reference to the floor) in configuration 2 at 20,000 G impact.

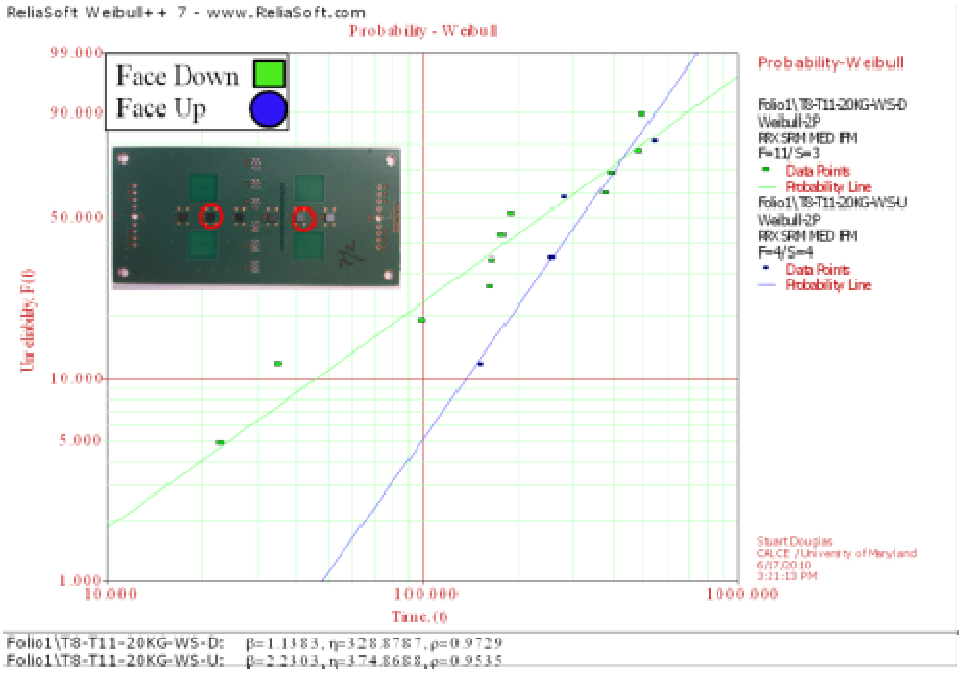

Figure 56: Comparison of middle component (T8 and T11) failure times with varying component orientation (in reference to the floor) in configuration 2 at 20,000 G impact.

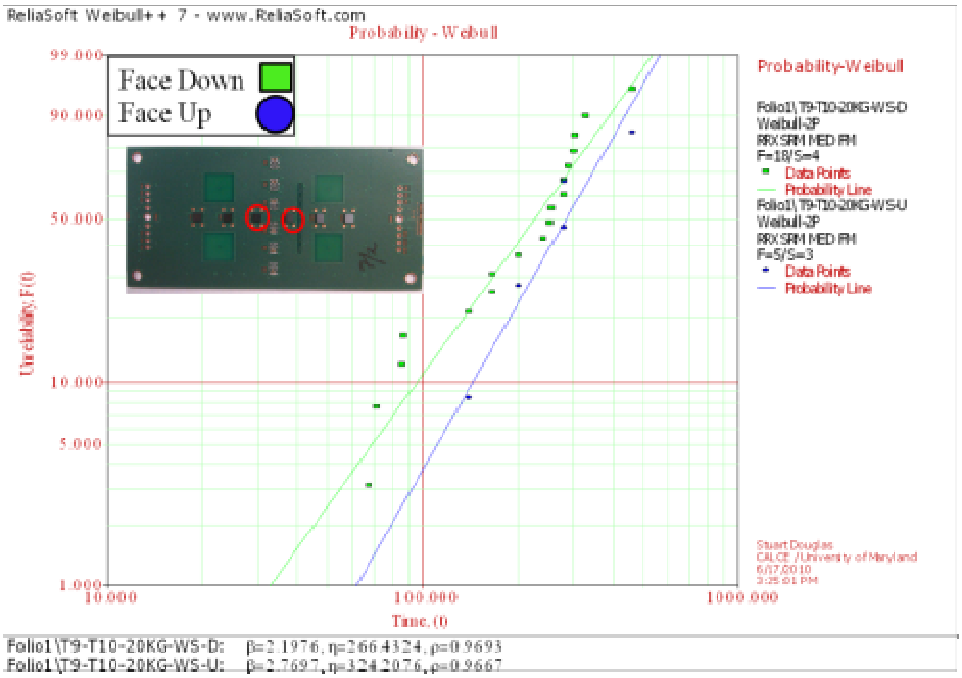

Figure 57 Comparison of inner component (T9 and T10) failure times with varying component orientation (in reference to the floor) in the configuration 2 at 20,000 G impact.

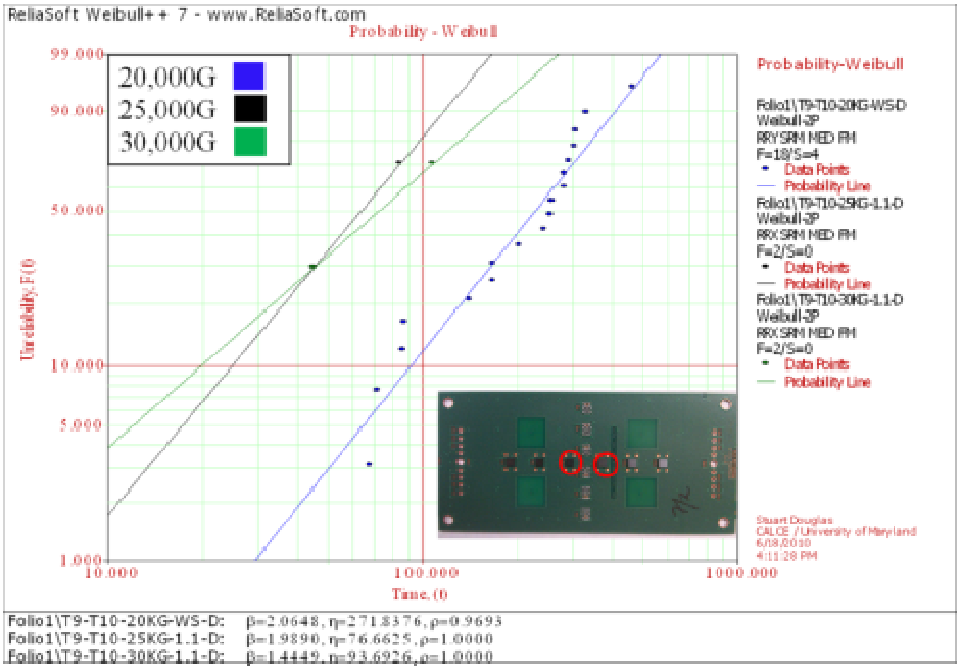

Figure 58: Comparison of inner components (T9 and T10), with component down orientation, failure times of boards in the configuration 2 at varying impact accelerations.

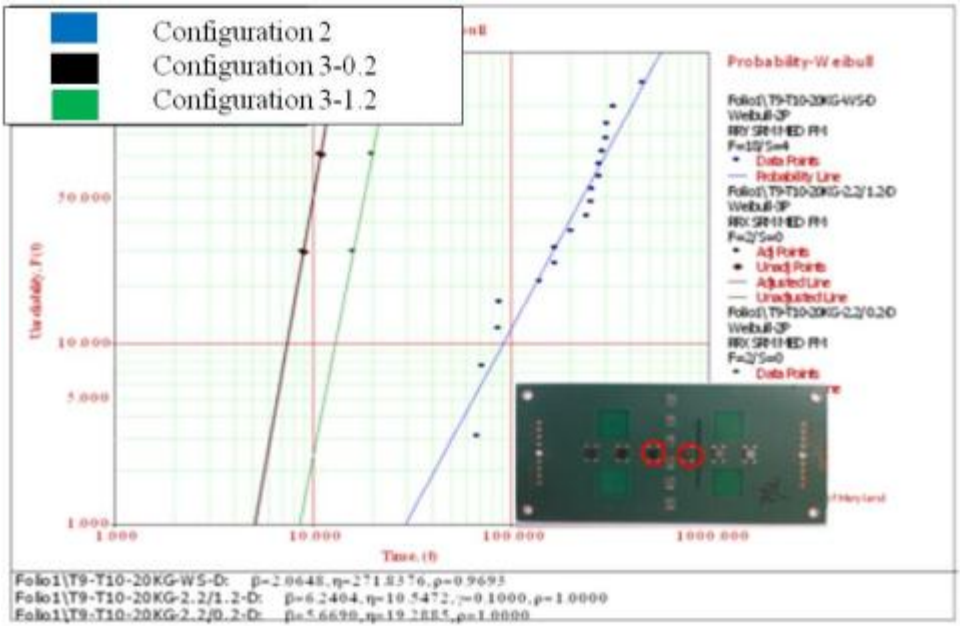

Figure 59: Comparison of inner components (T9 and T10), with component down orientation, failure times of boards in varying fixture types at a 20,000 G impact.

Appendix III Matlab Code

```
%Drop Tower analytical model
g = 9.8%m/s
Cr = 0.9
d = 0.21%m
m = 10%kg mass of the DMSA table
M = 80%kg mass of the drop table with DMSA base

%Starting from rest before
%Large Mass
y0 = 1%m
tti = sqrt(y0*2/g);%s
td = 0:0.0001:tti;%s
yM = -g*td.^2/2+y0;%m
vMi = -g*td;%m/s
ami = -g%initial accleration of the mass
%Small mass
ym = -g*td.^2/2+y0+d;%m
vmii = -g*td;%m/s


plot(td,yM,'g')
hold on
plot(td,ym)


%During impact of the large mass with Delrin
%Large mass
vMf = -vMi(length(vMi))*Cr%m/s
vmi = vmii(length(vmii))
%Calculation of time to impact of the two masses
ttim = -d/(vmi-vMf)%s
%Determining the duration b/w impacts
tai =td(length(td)):0.0001:ttim+td(length(td));%s
vMai = -g*tai+vMf+g*sqrt(2*y0/g);
yMai1 = -g/2.*tai.^2;%m
yMai2 = (vMf+g*sqrt(2*y0/g)).*tai;%m
yMai3 = -y0-vMf*sqrt(2*y0/g);%m
% y01=-vMf*sqrt(2*y0/g)
yMai = yMai1+yMai2+yMai3;

%Small mass continues to fall after the impact b/w the large mass and the
%Delrin
vmai = -g.*tai;%m/s
ymai = -g*tai.^2/2+y0+d;%m
hold on
plot(tai,yMai,'g')
hold on
title('Displacement of the DMSA system during a drop','FontWeight','bold','FontSize',30)
xlabel('Time (s)','FontWeight','bold','FontSize',30);
ylabel('Displacement (m)','FontWeight','bold','FontSize',30);
legend('DMSA base','DMSA table')
```

```
plot(tai,ymai)

%Impact between the masses
vmin = vmai(length(vmai));%m/s the intial velocity of the small mass
vMin = vMai(length(vMai));%m/s the intial velocity of the large mass
%Calculating the final velocities of the masses
vmf = (m*vmin+M*vMin - M*(Cr*(vmin-vMin)))/(m+M);
vMf = Cr*(vmin-vMin)+vmf;
%collecting the time
ti = tai(length(tai));
y01 = ymai(length(ymai));
Y01 = yMai(length(yMai));
tinf = tai(length(tai)):0.001:1;

%end velocity of small mass
vinf = -g.*tinf+vmf+g*ti;
yinf = -g.*tinf.^2/2 + (vmf + g*ti).*tinf + y01+g*ti^2/2-(vmf+g*ti)*ti;
%end velocity of large mass
vINF = -g.*tinf+vMf+g*ti;
yINF = -g.*tinf.^2/2 + (vMf + g*ti).*tinf + Y01+g*ti^2/2-(vMf+g*ti)*ti;

hold on
plot(tinf,yinf)
hold on
plot(tinf,yINF,'g')

figure
plot(td,vMi,'r-')
hold on
plot(td,vmii,'b-')
hold on
plot(tai,vMai,'r-')
hold on
plot(tai,vmai,'b-')
hold on
plot(tinf,vINF,'r-')
hold on
title('Velocity of the DMSA system during a drop','FontWeight','bold','FontSize',30)
xlabel('Time (s)','FontWeight','bold','FontSize',30);
ylabel('Velocity (m/s)','FontWeight','bold','FontSize',30);
legend('DMSA base','DMSA table')
plot(tinf,vinf,'b-')
```

References

[1] Goyal, S., Upsani, S. and Patel, D.M., "Improving impact toleratnce of portable electronic products: Case study of cellular phones." Experimental Mechanics, 1999, Issue 1, Vol. 39, pp. 43-52.

[2] Askari, A. F., Al-Bassyiouni, M. and Dasgupta, A., "Shock and Dynamic Loading in Portable Electronic Assemblies: Modeling and Simulation Results." Journal of Electronic Packaging, 2010.

[3] Hart, J. B. and Herrmann, R. B., "Energy Transfer in One-Dimensional Collisions of Many Objects." American Journal of Physics, 1968, Vol. 36, pp. 46-48.

[4] Rodgers, B., Goyal, S. and Sheehy, M., "The Dynamics of Multiple Pair-wise Collisions in a Chain for Designing Optimal Shock Amplifiers." Shock and Vibration, 2009, Vol. 16, pp. 99-116.

[5] Kerwin, J. D., "“Velocity, Momentum, and Energy Transmissions in Chain Collisions." American Jounal of Physics, 1972, Vol. 40, pp. 1152-1157.

[6] Harter, W. G., "Velocity Amplification in Collision Experiments Involving Superballs." American Journal of Physics, 1971, Vol. 39, pp. 656-663.

[7] Rodgers, B., et al., "The Dynamics of Shock Amplification." London : U.K., 2008. Proc. of the World Congress on Engineering.

[8] Kelly, G., et al., "Shock Pulse Shaping in a Small-form Factor Velocity Amplifier." Shock and Vibration, 2009, Vol. 16, pp. 1-17.

[9] JEDEC Solid State Technology Association., *JESD22-B111: Board Level Drop Test Method of Component for Handheld Electronic Products.*

[10] Shan, H., et al., "Multiple Impact Dynamics of a Falling Rod and its Numerical Solution." Orlando : Fl, 2004. The 8th International Conf. on Integral Methods in Science and Engineering.

[11] Shan, H., et al., "Modeling and Simulation of Multiple Impacts of Falling Rigid Bodies." Mathematics and Computer Modelling, 2006, Vol. 43, pp. 592-611.

[12] Shan, H., et al., "Three Dimensional Modeling and Simulation of a Falling Electronic Device." Asme Journal of Computational and Nonlinear Dynamics, 2006, Issue 1, Vol. 2, pp. 22-31.

[13] Douglas, S., Al-Bassyiouni, M. and Dasgupta, A., "Simulation of Drop Testing at Extremely High Accelerations." Bordeaux : Fr, 2010. EuroSimE IEEE Conference.

[14] Nummila, P., Johansson, M. and Puro, S., "Mechanical Shock Robustness of Different WLCSP Types." 2008. Electronic Components and Technology Conference. pp. 1963-1969.

[15] Chen, K. M., Ho, K. K. and Jiang, D. S., "Impact of Lead Free Solder Materials on Board Level Reliability for Low-K WLCSP." 2007. Microsystems, Packaging, Assembly and Circuits Technology, IMPACT International. pp. 243-245.

[16] Alajoki, M., Nguyen, L. and Kivilahti, J., "Drop Test Reliability of Wafer Level Chip Scale Packages." 2005. Electronic Components and Technology Conference. Vol. 55, pp. 637-644.

[17] Xueren, Z., et al., "Study on Board Level Drop Reliability of Wafer Level Chip Scale Package with Leadfree Solder." 2008. Electronics Packaging Technology Conference. pp. 1096-1101.

[18] Shea, H. R., "Reliability of MEMS for Space Applications." San Jose : Ca, 2006. Proc. of SPIE. Vol. 6111.

[19] Sheehy, M., et al., "The Failure Mechanisms of Micro-scale Cantilevers in Shock and Vibration Stimuli." Journal of Microelectromechanical Systems, 2002, Issue 3, Vol. 11, pp. 206-214.

[20] Pissano, A. P., "MEMS and Nano Technology for the Handheld, Portable Electronic and the Automotive Markets, Solid State Sensor." s.l. : Transducers International, 2007. Actuators and Microsystems Conference.

[21] Wong, E. H., Mai, Y. W. and Woo, M., "Analytical Solution for the Damped-Dynamics of Printed Circuit Board and Applied to Study the Effects of Distorted Half-Sine Support Excitation." IEEE Transactions on Advanced Packaging, 2009, Issue 2, Vol. 32, pp. 536-545.

[22] Dukkipati, Rao V., *Vibration Analysis.* Middlesex : Alpha Science Internation LTD, 2004.

[23] Abaqus Inc., "Volume V: Prescribed Conditions, Constraints and Interactions." *Analysis Users' Manual.* 2003.

[24] Goyal, S., Papadopolous, J. M. and Sullivan, P. A., "The Dynamics of Clattering I: Equation of Motion and Examples." Journal of Dynamic Systems, Measurements, and Control, 1998, Vol. 120, pp. 83-93.

[25] Mindlin, R. D., ""“Dynamics of Package Cushioning." Bell Systems Technology Journal, 1946, pp. 424-426.

[26] Newton, R. E., "Theory of Shock Isolation." *Shock & Vibration Shock & Vibration Handbook.* New York : McGraw-Hill, 31.

[27] Goyal, S., Papadopolous, J. M. and Sullivan, P. A., "Shock Protection of Portable Electronic Products: Shock Response Spectrum, Damage Boundary Approach, and Beyond." Shock and Vibration, New York : s.n., 1997, Issue 3, Vol. 4, pp. 169-191.

[28] Varghese, J., *Drop Testing of Portable Electronic Devices.* Mechanical Engineering, University of Maryland. College Park : University of Maryland, 2006. Ph. D. Thesis.

[29] Wong, E. H., et al., "Drop Impact: Fundamentals and Impact Characterisation of Solder Joints." Lake Buena Vista : Fl, 1202-1209. Proc. Electronic Components and Technology Conference.